frontiers | Frontiers in Materials

TYPE Original Research
PUBLISHED 15 December 2022
DOI 10.3389/fmats.2022.1055397

OPEN ACCESS

EDITED BY
Haitao Wang,
Hohai University, China

REVIEWED BY
Lokman Gemi,
Necmettin Erbakan University, Turkey
Fethi Abbassi,
American University of the Middle East, Kuwait

*CORRESPONDENCE
Haytham F. Isleem,
isleemhaytham88@gmail.com

SPECIALTY SECTION
This article was submitted to Structural Materials,
a section of the journal
Frontiers in Materials

RECEIVED 27 September 2022
ACCEPTED 02 November 2022
PUBLISHED 15 December 2022

CITATION
Isleem HF, Jagadesh P, Qaidi S, Althoey F, Rahmawati C, Najm HM and Sabri MMS (2022), Finite element and theoretical investigations on PVC–CFRP confined concrete columns under axial compression.
Front. Mater. 9:1055397.
doi: 10.3389/fmats.2022.1055397

Finite element and theoretical investigations on PVC–CFRP confined concrete columns under axial compression

Haytham F. Isleem[1]*, P. Jagadesh[2], Shaker Qaidi[3,4], Fadi Althoey[5], Cut Rahmawati[6], Hadee Mohammed Najm[7] and Mohanad Muayad Sabri Sabri[8]

[1]Department of Construction Management, Qujing Normal University, Qujing, Yunnan, China, [2]Department of Civil Engineering, Coimbatore Institute of Technology, Coimbatore, Tamil Nadu, India, [3]Department of Civil Engineering, College of Engineering, University of Duhok, Duhok, Iraq, [4]Department of Civil Engineering, College of Engineering, Nawroz University, Duhok, Iraq, [5]Department of Civil Engineering, College of Engineering, Najran University, Najran, Saudi Arabia, [6]Department of Civil Engineering, Universitas Abulyatama, Aceh Besar, Indonesia, [7]Department of Civil Engineering, Zakir Husain Engineering College, Aligarh Muslim University, Aligarh, India, [8]Peter the Great St. Petersburg Polytechnic University, Petersburg, Russia

This article examines the performance of Carbon Fibre Reinforced Polymer (CFRP) on Concrete Filled with Polymer Vinyl Chloride Tube (CFPT) columns under axial compression. Firstly, 44 CFPT specimens from the literature were analyzed using ABAQUS software to understand the compressive behavior of specimens under applied displacement. Secondly, 268 CFPT specimens are simulated to understand the influence of CFRP on these control specimens with a varying number of FRP layers and wrapping depth. Other variables such as the unconfined concrete strength, the thickness of the PVC tube, and the size and slenderness ratio of the columns were also studied. Studies are extended to confinement damage plasticity model analysis of CFRP-CFPT (CCFPT) columns. Relationships between the load-carrying capacity of CCFPT columns and the CFRP properties were developed. The effect of these parameters on the CFPT leads to the development of analytical models. It is an advantage to applying a such new type of composite columns in various applications.

KEYWORDS

ABAQUS, concrete filled PVC tubes, load carrying capacity, finite element model, damage plasticity model

Highlights

- Axial compression behavior of concrete-filled CFRP–PVC tubular (CFCT) columns.
- A confined damage plasticity model for finite element model (FEM) simulation of the CFCT column was developed.
- Effect of column test variables

- Model development to predict the failure strength and strain of CFCT columns.

1 Introduction

The usage of composite materials like concrete-filled steel tubes results in long-term strength and poor durability characteristics (Han et al., 2014). To overcome this, research recommends the usage of plastics. One such kind is Polymer Vinyl Chloride (PVC) materials which demonstrate extraordinary mechanical properties related to other general plastics, establishing a remarkable ratio of cost to performance, and specifically amazing durability (Wang and Yang, 2010). Several authors (Abbassi and Ahmad., 2020; Kazmi et al., 2021) even introduced waste materials for making composite materials having enhanced mechanical properties. Nowack et al. (1995) investigated the usage of soil-buried PVC pipes excavated up after 60 years of active use, which showed no deterioration and were expected to have an additional useful life of 50 years. There are several advantages like high strength, high stiffness, higher confinement strength, and full usage of materials used in composite columns like Concrete Filled PVC Tubes (CFPT) columns in various applications. Therefore, the number of researchers who studied, concrete columns confined by different materials (Guo et al., 2008) is increased and the inclusion of such composite material can increase the ultimate strength and strain of concrete (Jiang et al., 2014) of composite columns. Vedernikov, et al., 2022 reported that the pulling speed significantly affects the morphology and mechanical properties of fiber composites for structural applications. The stiffness and load-carrying capacities of a beam are enhanced by wrapping different types of fibers. And also, the study is extended to the effect of fully and partially wrapping fibers on the load-carrying capacity and stiffness (Gemi et al., 2022a). Aksoylu, et al. (2022) proved that the different FRP profiles of FRP boxes, strengthened by FRP wrapping enhance the compressive strength of composites.

CFPT columns exposed to the severe environmental condition indicated that no degradation in the strength and ductility of the specimen is reported by Gupta and Verma. (2014). Even CFPT columns submerged in seawater for 6 months revealed that the microstructure of infilled concrete and the chemical composition of PVC remains unaltered (Gupta and Verma., 2014). PVC tubes subjected to accelerated aging in the air at 80°C and 90°C for 8 weeks suffered no important changes in mechanical properties and elongation at fracture of PVC materials (Jackubowicz et al., 1999). Apart from durability characteristics usage of PVC tubes increases the load-carrying capacity of a column and also increases the longitudinal deformation capacity. Although there are a lot of advantages are there in utilizing CFPT columns for various applications, it also has several disadvantages. CFPT columns can efficiently inhibit the interior buckling of the PVC tube. Deformation and failure of CFPT are caused primarily by the peripheral buckling of the PVC tube.

Wrapping of Fiber Reinforced Polymer (FRP) material outside the concrete-filled tube can restrain the local buckling (Xiao., 2004). In addition, FRP increases the confinement strength by compensating for the weak confinement provided by PVC tubes, introducing confined CFPT columns. One such FRP used in this investigation is Carbon Fibre Reinforced Polymer (CFRP), which is used for wrapping around the CFPT columns thereby enhancing the mechanical and durability properties. CFRP has several advantages such as high strength, good durability, fatigue resistance, and light weight (Yu et al., 2019). It is also noted that the usage of CFRP composites as externally bonded reinforcement for the retrofit of structures become popular among researchers and in the construction sector (Jiang et al., 2014). The introduction of FRP in concrete-filled tubular columns provides superior behavior such as corrosion resistance, good ductility, and comfort for construction have been confirmed by Teng et al., 2007. The introduction of fibers, as well as the wrapping of the specimens, will increase the enhanced properties as reported by (Hadi., 2009). It is also reported that the full wrapping of CFRP results in high cost. Even a few scholars proposed to solve the above problems by partially wrapping CFRP in concrete-filled PVC tubes. (e.g., Harajli., 2006; Ping and Peng., 2006; Yu., 2007).

Composite columns proposed in this study that are CFPT specimens are either fully or partially wrapped by CFRP, shell confining the core concrete. This composite system is lightweight, cost-effective, enhanced load-carrying capacity axially and laterally, and provides superior durability characteristics, which allows a possible suggestion for its applications in pile foundations and bridge piers in a severe environment subjected to seawater conditions. It is reported in the literature that the most of costs are spent on maintaining piling systems and repairing concrete piers. The usage of CFPT columns wrapped by CFRP is regarded as a promising approach to overcoming this problem (Zhang and Hadi., 2020; Micelli, et al., 2015). Concrete-filled FRP tubes exhibit higher ductility this is because of the high strain enhancement ratio noted (Ozbakkaloglu and Vincent., 2014) and it is expensive. CFPT and the external confinement provided by continuous impregnated FRP hoops that may have various spacings were investigated by Toutanji and Sennah., 2002. This kind of hybrid column improves both the failure strain and strength of the concrete. FRP-confined CFPT columns have higher ultimate strain and strength as reported by Fakharifar and Chen (2016).

Wang et al. (2012a) tested cyclic compressive load on two square RC columns of sizes 204 × 204 × 612 mm and 305 × 305 × 915 mm. Enhancement of axial compressive strength capacity due to steel confinement reinforcement is reported. It is also stated that the longitudinal and hoop reinforcement is influenced by the shape of stress-strain curves, loading/reloading paths, and

plastic strain. Masia et al. (2004) investigated three different square section sizes (100, 125, and 150 mm) on the FRP evaluated. FRP confinement decreases with increases in cross-sectional size. There is a difference in axial stress-strain responses for the different sizes was confirmed by (Rocca., 2007). The contribution of hoop reinforcement to compressive strength enhancement was reported by Isleem et al. (2018a). It is also reported that the internal hoop steel reinforcing bars were found to be mostly dependent on the cross-sectional size and number of CFRP layers. Isleem et al. (2018a) also extended the effect of steel reinforcement on the strain and loading path of axially loaded columns.

Effect of the internal longitudinal, hoop steel reinforcement and cross-sectional size on the stress-strain behavior of CFRP confined unreinforced and reinforced columns subjected to axial load (Wang et al., 2012b). Results show that the efficiency of confinement is decreased as the cross-sectional sizes increase. Influence of internal longitudinal and hoop steel reinforcement on the compressive strength enhancement as reported by Isleem et al. (2018b). PVC tubes wrapped by FRP provided lateral confinement and created triaxial stress in the concrete, which constrained concrete during dilation and consequently, enhanced its capacity of load bearing when the height-to-diameter ratio is 3 (Toutanji and Sennah 2002). The compressive strength of FRP-confined CFPT columns is based on the fiber type and hoop spacing used externally. CFPT columns with various PVC thicknesses wrapped by two different types of fibers CFRP and GFRP with a height-to-diameter ratio of 2:1 investigated by Mammen and Antony. (2017). They also extended their investigations to two dissimilar patterns of circular and helical wrapping with two different ways of reducing the hoop spacing between FRP. Higher strength was noted for the CFRP circular wrapping with larger PVC thickness. The enhancement of strength and ductility nature of CFPT columns with FRP wraps in which fibers are oriented in the hoop direction was reported by (Fakharifar and Chen, 2017). The higher value of FRP tube thickness or strip used to wrap CFPT leads to a higher improvement in strength and deformation (Gao et al., 2019).

A lot of studies revealed that many advantages of the usage of this kind of composite columns, the interaction and relation models between Concrete, PVC, reinforcement, and CFRP have not been analytically reported. In literature, it is reported that the use of CFRP-confined CFPT column increases the structural performance of concrete; however, the effect of several parameters like concrete compressive strength, PVC tube thickness, column slenderness ratio, and specimen size on the stress and strain of those columns are not exposed properly. There is also no proper discussion about the effect of the CFRP behaviors like thickness, the number of layers, and depth of CFRP wrapping on above said parameters.

1.1 Research significance

This study aimed to investigate analytically the structural performance of CFRP-confined CFPT columns. In the literature, limited studies are available on the effect of confined concrete strength, PVC tube thickness, slenderness ratio, and specimen size on the failure axial load of CFPT columns wrapped with CFRP. However, there are several models available in the literature to estimate the ultimate axial load of CFPT columns without CFRP wrappings. These models are mostly used to estimate the ultimate axial load from confined concrete strength and lateral confining pressure for CFPT columns. Hence, it is necessary to develop a model by considering all these parameters in terms of dimensionless parameters to estimate the failure axial load of CFPT columns wrapped by CFRP. For this purpose, FE simulations are required and the results obtained are compared with experimental results from literature for CFPT columns alone initially. And simulations are extended towards the CFRP-confined CFPT columns.

1.2 Research scope

The objective of this study is to numerically estimate the influencing parameters on the behavior of concrete-filled composite tubes under concentric load. First, the experimental CFPT specimens from the literature are simulated by ABAQUS software (ABAQUS, 2014), and the simulated results like stress-strain curve, failure axial load, and failure modes are compared with experimental results. Secondly, the simulation is extended towards the same CFPT columns partially/fully wrapped by CFRP and simulated results are evaluated. The influence of internal steel reinforcement, unconfined concrete strength, slenderness ratio, specimen size and thickness of PVC tube on load carrying capacity, and strain of CFPT column was investigated. And the study is further extended to the impact of CFRP behaviors (Thickness of CFRP, number of layers of CFRP, and depth of CFRP wrapping) on above said parameters for CCFPT columns are examined.

2 Experimental data base

The first part of the simulated experimental work includes the comparison of the simulated stress-strain model of CFPT columns from the experimental work. A wide-ranging database with a test result of 44 CFPT columns with different unconfined concrete strength, the thickness of PVC tubes, slenderness ratios, and specimen sizes were collected from 8 different studies (Feng and Ditao, 2013; Fang et al., 2020; Chang et al., 2021; Bandyopadhyay et al., 2019; Woldemariam et al., 2019; Alatshan et al., 2022; Gupta, 2013). Experimental stress and strain value from literature for 44 CFPT columns are

TABLE 1 Summary of confined concrete filled PVC tube without CFRP.

S.No	Code	Author	Size: D x H x t	D_c	f_c'	Reinforcement	ε_{EP}	ε_{FP}	P_{EP}	P_{FP}	
			(mm) x (mm)	mm	MPa	Longitudinal	Hoop	mm/mm	mm/mm	kN	kN
1	E01	Fang et al. (2020)	200 × 500 × 7.8	184.4	28.50	0	0	0.0117	0.0117	972.300	935.234
2	E02	Feng and Ditao (2013)	200 × 500 × 7.8	184.4	28.50	10Ø110	6Ø104	0.0117	0.0117	-	-
3	E03	Chang et al. (2021)	168 × 588 × 5.0	158.0	34.13	0	0	0.0094	0.0119	651.522	692.922
4	E04	Bandyopadhyay et al. (2019)	160 × 500 × 2.3	155.4	31.30	10Ø110	6Ø104	0.0049	0.0054	783.500	775.380
5	E05	Bandyopadhyay et al. (2019)	160 × 500 × 3.7	152.6	31.30	10Ø110	6Ø104	0.0065	0.0079	826.500	789.345
6	E06	Bandyopadhyay et al. (2019)	160 × 500 × 5.4	149.2	31.30	10Ø110	6Ø104	0.0084	0.0108	838.000	832.456
7	E07	Bandyopadhyay et al. (2019)	160 × 1000 × 2.3	155.4	31.30	10Ø110	6Ø104	0.0049	0.0054	721.500	726.726
8	E08	Bandyopadhyay et al. (2019)	160 × 1000 × 3.7	152.6	31.30	10Ø110	6Ø104	0.0065	0.0079	759.500	753.671
9	E09	Bandyopadhyay et al. (2019)	160 × 1000 × 5.4	149.2	31.30	10Ø110	6Ø104	0.0084	0.0108	808.000	796.359
10	E10	Bandyopadhyay et al. (2019)	160 × 1000 × 2.3	155.4	36.40	10Ø110	6Ø104	0.0047	0.0050	809.500	798.143
11	E11	Bandyopadhyay et al. (2019)	160 × 1000 × 3.7	152.6	36.40	10Ø110	6Ø104	0.0060	0.0072	810.500	819.311
12	E12	Bandyopadhyay et al. (2019)	160 × 1000 × 5.4	149.2	36.40	10Ø110	6Ø104	0.0077	0.0098	864.500	875.965
13	E13	Bandyopadhyay et al. (2019)	160 × 750 × 2.3	155.4	31.30	10Ø110	6Ø104	0.0049	0.0054	755.500	748.143
14	E14	Bandyopadhyay et al. (2019)	160 × 750 × 3.7	152.6	31.30	10Ø110	6Ø104	0.0065	0.0079	807.000	763.428
15	E15	Bandyopadhyay et al. (2019)	160 × 750 × 5.4	149.2	31.30	10Ø110	6Ø104	0.0084	0.0108	837.000	802.379
16	E16	Woldemariam et al. (2019)	63 × 126 × 2.5	58.0	10.50	0	0	0.0211	0.0209	75.990	84.004
17	E17	Woldemariam et al. (2019)	90 × 180 × 3.0	84.0	10.50	0	0	0.0181	0.0178	147.250	149.004
18	E18	Woldemariam et al. (2019)	110 × 220 × 3.0	104.0	10.50	0	0	0.0152	0.0147	209.070	195.734
19	E19	Woldemariam et al. (2019)	140 × 280 × 3.0	134.0	10.50	0	0	0.0125	0.0116	323.140	277.802
20	E20	Woldemariam et al. (2019)	63 × 126 × 2.5	58.0	13.79	0	0	0.0170	0.0169	85.630	90.309
21	E21	Woldemariam et al. (2019)	90 × 180 × 3.0	84.0	13.79	0	0	0.0147	0.0143	170.470	159.691
22	E22	Woldemariam et al. (2019)	110 × 220 × 3.0	104.0	13.79	0	0	0.0124	0.0118	235.690	215.149
23	E23	Woldemariam et al. (2019)	140 × 280 × 3.0	134.0	13.79	0	0	0.0103	0.0093	365.690	305.374
24	E24	Woldemariam et al. (2019)	63 × 126 × 2.5	58.0	16.89	0	0	0.0146	0.0144	89.530	96.237
25	E25	Woldemariam et al. (2019)	90 × 180 × 3.0	84.0	16.89	0	0	0.0126	0.0122	181.190	171.900
26	E26	Woldemariam et al. (2019)	110 × 220 × 3.0	104.0	16.89	0	0	0.0108	0.0100	256.500	234.223
27	E27	Woldemariam et al. (2019)	140 × 280 × 3.0	134.0	16.89	0	0	0.0090	0.0078	378.180	327.540
28	E28	Woldemariam et al. (2019)	63 × 126 × 2.5	58.0	20.13	0	0	0.0128	0.0125	100.140	101.846
29	E29	Woldemariam et al. (2019)	90 × 180 × 3.0	84.0	20.13	0	0	0.0112	0.0105	195.170	187.107
30	E30	Woldemariam et al. (2019)	110 × 220 × 3.0	104.0	20.13	0	0	0.0096	0.0086	281.850	250.976
31	E31	Woldemariam et al. (2019)	140 × 280 × 3.0	134.0	20.13	0	0	0.0080	0.0067	431.180	363.076
32	E32	Woldemariam et al. (2019)	63 × 126 × 2.5	58.0	24.12	0	0	0.0113	0.0107	108.250	109.618
33	E33	Woldemariam et al. (2019)	90 × 180 × 3.0	84.0	24.12	0	0	0.0099	0.0091	218.290	201.497
34	E34	Woldemariam et al. (2019)	110 × 220 × 3.0	104.0	24.12	0	0	0.0085	0.0074	311.380	274.362
35	E35	Woldemariam et al. (2019)	140 × 280 × 3.0	134.0	24.12	0	0	0.0072	0.0057	475.160	417.995
36	E36	Alatshan et al. (2022)	70 × 158 × 2.0	66.0	15.00	0	0	0.0091	0.0075	73.200	66.229
37	E37	Alatshan et al. (2022)	100 × 225 × 3.0	94.0	15.00	0	0	0.0096	0.0081	144.100	126.331
38	E38	Alatshan et al. (2022)	150 × 338 × 3.0	144.0	15.00	0	0	0.0071	0.0053	257.800	271.573
39	E39	Alatshan et al. (2022)	70 × 158 × 2.0	66.0	35.00	0	0	0.0057	0.0035	128.700	131.241
40	E40	Alatshan et al. (2022)	100 × 225 × 3.0	94.0	35.00	0	0	0.0059	0.0038	259.400	260.693
41	E41	Gupta (2013)	140 × 500 × 3.9	132.2	28.60	0	0	0.0072	0.0049	511.000	515.973
42	E42	Gupta (2013)	160 × 500 × 4.25	151.5	23.60	0	0	0.0076	0.0053	639.600	584.727
43	E43	Gupta (2013)	140 × 500 × 3.9	132.2	43.50	0	0	0.0060	0.0034	742.000	739.937
44	E44	Gupta (2013)	165 × 495 × 4.0	157.0	33.60	0	0	0.0074	0.0096	417.000	432.914

D: Diameter of circular section (mm), H: Height of specimen (mm), D_c: Diameter of the concrete core without PVC, tube (mm), f_c': strength of unconfined concrete cylinder under compression (MPa), ε_{EP}: Peak experimental strain (mm/mm), ε_{FP}: Peak finite element modeling strain (mm/mm), P_{EP}: Peak Experimental Load (kN), P_{FP}: Peak finite element modeling Load (kN).

stipulated using ABAQUS software (ABAQUS, 2014) and compared with simulated stress and strain (Isleem et al., 2022). The summary of controlled specimens used in these investigations are these 44 CFPT specimens and their results are tabulated in Table 1.

The study is extended further to develop simulated CFPT columns wrapped with fully/partially CFRP using ABAQUS software (ABAQUS, 2014). Table 2 provides the summary of the CFRP-wrapped CFPT columns. The parameters varied are thickness, depth, and the number of layers of CFRP on the load-carrying capacity of the column. Based on the CFRP properties, the entire research work is grouped into twelve groups based on the CFRP depth and number of layers of CFRP, for controlled specimens. The depth of CFRP layers varies from 20, 30, 40, 50, 60, and 100 mm in group 1. With an increase in CFRP depth, there is a decrease in load-carrying capacity is noted. With an increase in the number of layers, the load-carrying capacity of columns increases is noted.

For group 2, for the same specimens, the CFRP total thickness and number of layers are varied, whereas the depth of CFRP is kept constant. With the increase in the number of layers, there is an increase in the load-carrying capacity of the specimen is observed. For group 3, the load-carrying capacity of CFPT columns increases with an increase in the number of layers, and the load-carrying capacity decreases with an increase in CFRP depth. Similar to group 3, group 4 has a similar load-carrying capacity behavior, but with the increase in confined concrete strength, an increase in load-carrying capacity is observed.

Group 5, shows that an increase in the number of layers increases the load-carrying capacity of CCFPT columns, whereas an increase in the depth of CFRP layers, results in a decrease in load-carrying capacity is observed. And also, an increase in the number of layers up to 40 mm depth of CFRP layers results in a decrease in the strain of CCFPT columns are noted, and after that, there is a decrease in strain value is decreased. With an increase in height of CCFPT columns, there is a decrease in load-carrying capacity for group 6 is noted, whereas an increase in confined concrete strength increases load-carrying capacity. There are three subgroups were noted for group 6, with two subgroups having different confined concrete strengths and the same height of columns whereas the third subgroup has different heights of columns with the same confined concrete strength.

For group 7, the parameters like PVC thickness, specimen height, number of layers, and CFRP depths are varied. The second highest ultimate strain value is noted in group 7 when compared to all other groups. There are two major subgroups are noted for group 8 with two different confined concrete compressive strengths. Each subgroup has three different subgroups based on the PVC thickness. Therefore, six subgroups are noted in group 8. With an increase in confined concrete strength, there an increase in the load-carrying capacity is observed. There are two major subgroups are noted for group 9 with two different confined concrete compressive strengths. There are three subgroups for the number of layers. In each sub-group, there is an increase in the depth of CFRP layers there is a decrease in load-carrying capacity is observed. With an increase in the number of layers, there is an increase in load-carrying capacity is noted. Similar to group 9, group 10 has the same trend but the PVC thickness is less. Two major groups are noted with group 10 but the behavior remains similar. The load-carrying capacity of columns increases with an increase in PVC thickness as noted in group 11 for layer 1, whereas for 3 layers the load-carrying capacity remains the same. Group 12 has four different depths of CFRP layers with an increase in depth resulting in a decrease in load-carrying capacity. An increase in PVC thickness results in an increase in the load-carrying capacity of the column is noted.

3 Finite element modelling

3.1 Element and interaction

3.1.1 Finite element type

The S4R shell element was used to model the hollow PVC tube, to accurately predict its deformation. The S4R element has six degrees of freedom at every node. However, the concrete core was simulated with a C3D8R element. Two rigid plates were modeled at the top and bottom of the composite column. The bottom plate was fixed, while the top rigid plate has the freedom to move downward to transfer axial load. Implementation of a good mesh size would lead to accurate calculation within a period.

3.1.2 Interface

The surface-to-surface contact model was employed to model the interactions between the external surface of the concrete core and the internal surface of the PVC tube. Meanwhile, hard contact interaction was utilized in the normal direction, which prevents compressive state penetration by the concrete and PVC elements. However, the interaction between the PVC and concrete was regarded as a "Tie" (Ozkilic et al., 2022). Two reference points RP1 and RP2 were attached to the rigid plates.

3.1.3 Boundary conditions and load applications

The reference point at the top rigid plate was set to have freedom of vertical displacement, while in the other directions freedom was constrained. The reference point at the bottom rigid plate was constrained in all degrees of freedom. The vertical displacement was modeled to simulate the axial loadings. For the eccentric load conditions, the axial load was applied at 20, 30, 40, and 50 away from the central axis.

TABLE 2 Summary of confined concrete filled PVC tube with CFRP.

S.No	Group code	Code	Size: D x H x t	D_c	f_c'	Reinforcement		CFRP			CFRP-depth	P_{FF}	ε_{FF}
			(mm) x (mm)	mm	MPa	Longitudinal	Hoop	No. Of layers	Thickness/ Layers mm	Total thickness mm	mm	kN	mm/ mm
45	G1	E45	200 × 500 × 7.8	184.4	28.5	0	0	1	0.165	0.165	20	1214.75	0.0158
46		E46	200 × 500 × 7.8	184.4	28.5	0	0	1	0.165	0.165	30	1146.39	0.0152
47		E47	200 × 500 × 7.8	184.4	28.5	0	0	1	0.165	0.165	40	1110.96	0.0148
48		E48	200 × 500 × 7.8	184.4	28.5	0	0	1	0.165	0.165	50	1086.16	0.0156
49		E49	200 × 500 × 7.8	184.4	28.5	0	0	1	0.165	0.165	60	1060.44	0.0143
50		E50	200 × 500 × 7.8	184.4	28.5	0	0	2	0.165	0.330	20	1480.34	0.0155
51		E51	200 × 500 × 7.8	184.4	28.5	0	0	2	0.165	0.330	30	1375.73	0.0162
52		E52	200 × 500 × 7.8	184.4	28.5	0	0	2	0.165	0.330	40	1289.05	0.0150
53		E53	200 × 500 × 7.8	184.4	28.5	0	0	2	0.165	0.330	50	1237.10	0.0166
54		E54	200 × 500 × 7.8	184.4	28.5	0	0	2	0.165	0.330	60	1188.53	0.0146
55		E55	200 × 500 × 7.8	184.4	28.5	0	0	3	0.165	0.495	20	1807.41	0.0168
56		E56	200 × 500 × 7.8	184.4	28.5	0	0	3	0.165	0.495	30	1604.01	0.0170
57		E57	200 × 500 × 7.8	184.4	28.5	0	0	3	0.165	0.495	40	1468.77	0.0152
58		E58	200 × 500 × 7.8	184.4	28.5	0	0	3	0.165	0.495	50	1385.34	0.0181
59		E59	200 × 500 × 7.8	184.4	28.5	0	0	3	0.165	0.495	60	1313.12	0.0148
60		E60	200 × 500 × 7.8	184.4	28.5	0	0	1	0.165	0.165	100	1016.74	0.0144
61		E61	200 × 500 × 7.8	184.4	28.5	0	0	2	0.165	0.330	100	1100.16	0.0145
62		E62	200 × 500 × 7.8	184.4	28.5	0	0	3	0.165	0.495	100	1179.74	0.0147
63	G2	E63	168 × 588 × 5.0	158.0	34.13	0	0	1	0.165	0.165	20	870.85	0.0153
64		E64	168 × 588 × 5.0	158.0	34.13	0	0	2	0.165	0.330	20	1021.06	0.0161
65		E65	168 × 588 × 5.0	158.0	34.13	0	0	3	0.165	0.495	20	1142.67	0.0162
66		E66	168 × 588 × 5.0	158.0	34.13	0	0	1	0.165	0.165	20	789.41	0.0165
67		E67	168 × 588 × 5.0	158.0	34.13	0	0	2	0.165	0.330	20	861.33	0.0184
68		E68	168 × 588 × 5.0	158.0	34.13	0	0	3	0.165	0.495	20	915.75	0.0193
69		E69	168 × 588 × 5.0	158.0	34.13	0	0	1	0.165	0.165	20	772.87	0.0149
70		E70		158.0	34.13	0	0	2	0.165	0.330	20	829.27	0.0153

(Continued on following page)

TABLE 2 (*Continued*) Summary of confined concrete filled PVC tube with CFRP.

S.No	Group code	Code	Size: D x H x t	D_c	f_c'	Reinforcement		CFRP			CFRP-depth	P_{FF}	ε_{FF}
			(mm) x (mm)	mm	MPa	Longitudinal	Hoop	No. Of layers	Thickness/ Layers mm	Total thickness mm	mm	kN	mm/ mm
			168 × 588 × 5.0										
71		E71	168 × 588 × 5.0	158.0	34.13	0	0	3	0.165	0.495	20	877.92	0.0155
72		E72	168 × 588 × 5.0	158.0	34.13	0	0	1	0.165	0.165	20	744.87	0.0152
73		E73	168 × 588 × 5.0	158.0	34.13	0	0	2	0.165	0.330	20	775.71	0.0159
74		E74	168 × 588 × 5.0	158.0	34.13	0	0	3	0.165	0.495	20	789.21	0.0164
75	G3	E75	140 × 500 × 3.9	132.2	28.60	0	0	1	0.165	0.165	20	664.38	0.0154
76		E76	140 × 500 × 3.9	132.2	28.60	0	0	2	0.165	0.330	20	827.82	0.0131
77		E77	140 × 500 × 3.9	132.2	28.60	0	0	3	0.165	0.495	20	1062.92	0.0155
78		E78	140 × 500 × 3.9	132.2	28.60	0	0	1	0.165	0.165	20	583.33	0.0155
79		E79	140 × 500 × 3.9	132.2	28.60	0	0	2	0.165	0.330	20	692.32	0.0148
80		E80	140 × 500 × 3.9	132.2	28.60	0	0	3	0.165	0.495	20	795.62	0.0139
81		E81	140 × 500 × 3.9	132.2	28.60	0	0	1	0.165	0.165	20	551.90	0.0147
82		E82	140 × 500 × 3.9	132.2	28.60	0	0	2	0.165	0.330	20	615.60	0.0147
83		E83	140 × 500 × 3.9	132.2	28.60	0	0	3	0.165	0.495	20	680.29	0.0142
84		E84	140 × 500 × 3.9	132.2	28.60	0	0	1	0.165	0.165	20	518.18	0.0150
85		E85	140 × 500 × 3.9	132.2	28.60	0	0	2	0.165	0.330	20	548.25	0.0145
86		E86	140 × 500 × 3.9	132.2	28.60	0	0	3	0.165	0.495	20	567.22	0.0145
87	G4	E87	140 × 500 × 3.9	132.2	43.50	0	0	1	0.165	0.165	20	787.57	0.0155
88		E88	140 × 500 × 3.9	132.2	43.50	0	0	2	0.165	0.330	20	964.42	0.0159
89		E89	140 × 500 × 3.9	132.2	43.50	0	0	3	0.165	0.495	20	1140.87	0.0152
90		E90	140 × 500 × 3.9	132.2	43.50	0	0	1	0.165	0.165	20	713.14	0.0156
91		E91	140 × 500 × 3.9	132.2	43.50	0	0	2	0.165	0.330	20	803.32	0.0155
92		E92	140 × 500 × 3.9	132.2	43.50	0	0	3	0.165	0.495	20	895.95	0.0144
93		E93	140 × 500 × 3.9	132.2	43.50	0	0	1	0.165	0.165	20	674.90	0.0160
94		E94	140 × 500 × 3.9	132.2	43.50	0	0	2	0.165	0.330	20	740.42	0.0149
95		E95		132.2	43.50	0	0	3	0.165	0.495	20	795.04	0.0141

(Continued on following page)

TABLE 2 (*Continued*) Summary of confined concrete filled PVC tube with CFRP.

S.No	Group code	Code	Size: D x H x t	D_c	f_c'	Reinforcement		CFRP			CFRP-depth	P_{FF}	ε_{FF}
			(mm) x (mm)	mm	MPa	Longitudinal	Hoop	No. Of layers	Thickness/ Layers mm	Total thickness mm	mm	kN	mm/ mm
			140 × 500 × 3.9										
96		E96	140 × 500 × 3.9	132.2	43.50	0	0	1	0.165	0.165	20	652.02	0.0154
97		E97	140 × 500 × 3.9	132.2	43.50	0	0	2	0.165	0.330	20	678.38	0.0149
98		E98	140 × 500 × 3.9	132.2	43.50	0	0	3	0.165	0.495	20	691.98	0.0147
99	G5	E99	160 × 500 × 4.25	151.5	30.00	0	0	1	0.165	0.165	20	773.87	0.0150
100		E100	160 × 500 × 4.25	151.5	30.00	0	0	2	0.165	0.330	20	1013.80	0.0153
101		E101	160 × 500 × 4.25	151.5	30.00	0	0	3	0.165	0.495	20	1243.30	0.0150
102		E102	160 × 500 × 4.25	151.5	30.00	0	0	1	0.165	0.165	20	687.87	0.0151
103		E103	160 × 500 × 4.25	151.5	30.00	0	0	2	0.165	0.330	20	818.53	0.0141
104		E104	160 × 500 × 4.25	151.5	30.00	0	0	3	0.165	0.495	20	958.58	0.0142
105		E105	160 × 500 × 4.25	151.5	30.00	0	0	1	0.165	0.165	20	651.05	0.0142
106		E106	160 × 500 × 4.25	151.5	30.00	0	0	2	0.165	0.330	20	729.86	0.0143
107		E107	160 × 500 × 4.25	151.5	30.00	0	0	3	0.165	0.495	20	809.41	0.0135
108		E108	160 × 500 × 4.25	151.5	30.00	0	0	1	0.165	0.165	20	613.39	0.0143
109		E109	160 × 500 × 4.25	151.5	30.00	0	0	2	0.165	0.330	20	648.49	0.0143
110		E110	160 × 500 × 4.25	151.5	30.00	0	0	3	0.165	0.495	20	685.96	0.0133
111	G6(P1)	E111	90 × 180 × 3.0	84.0	10.50	0	0	1	0.165	0.165	180	427.23	0.0174
112		E112	90 × 180 × 3.0	84.0	10.50	0	0	2	0.165	0.330	180	717.77	0.0203
113		E113	90 × 180 × 3.0	84.0	10.50	0	0	3	0.165	0.495	180	1016.14	0.0233
114		E114	90 × 180 × 3.0	84.0	10.50	0	0	1	0.165	0.165	20	275.63	0.0146
115		E115	90 × 180 × 3.0	84.0	10.50	0	0	2	0.165	0.330	20	410.95	0.0158
116		E116	90 × 180 × 3.0	84.0	10.50	0	0	3	0.165	0.495	20	519.45	0.0158
117		E117	90 × 180 × 3.0	84.0	10.50	0	0	1	0.165	0.165	20	202.68	0.0140
118		E118	90 × 180 × 3.0	84.0	10.50	0	0	2	0.165	0.330	20	232.71	0.0131
119		E119	90 × 180 × 3.0	84.0	10.50	0	0	3	0.165	0.495	20	257.78	0.0124
120	G6(P2)	E120	90 × 180 × 3.0	84.0	24.12	0	0	1	0.165	0.165	180	452.63	0.0171

(Continued on following page)

TABLE 2 (*Continued*) Summary of confined concrete filled PVC tube with CFRP.

S.No	Group code	Code	Size: D x H x t	D_c	f_c'	Reinforcement		CFRP			CFRP-depth	P_{FF}	ε_{FF}
			(mm) x (mm)	mm	MPa	Longitudinal	Hoop	No. Of layers	Thickness/ Layers mm	Total thickness mm	mm	kN	mm/ mm
121		E121	90 × 180 × 3.0	84.0	24.12	0	0	2	0.165	0.330	180	709.71	0.0188
122		E122	90 × 180 × 3.0	84.0	24.12	0	0	3	0.165	0.495	180	1007.07	0.0219
123		E123	90 × 180 × 3.0	84.0	24.12	0	0	1	0.165	0.165	20	310.41	0.0147
124		E124	90 × 180 × 3.0	84.0	24.12	0	0	2	0.165	0.330	20	420.56	0.0151
125		E125	90 × 180 × 3.0	84.0	24.12	0	0	3	0.165	0.495	20	536.86	0.0157
126		E126	90 × 180 × 3.0	84.0	24.12	0	0	1	0.165	0.165	20	241.71	0.0142
127		E127	90 × 180 × 3.0	84.0	24.12	0	0	2	0.165	0.330	20	255.79	0.0139
128		E128	90 × 180 × 3.0	84.0	24.12	0	0	3	0.165	0.495	20	264.83	0.0131
129	G6(P3)	E129	110 × 220 × 3.0	104.0	10.50	0	0	1	0.165	0.165	220	535.57	0.0166
130		E130	110 × 220 × 3.0	104.0	10.50	0	0	2	0.165	0.330	220	885.24	0.0188
131		E131	110 × 220 × 3.0	104.0	10.50	0	0	3	0.165	0.495	220	1244.53	0.0213
132		E132	140 × 280 × 3.0	134.0	10.50	0	0	1	0.165	0.165	280	707.61	0.0157
133		E133	140 × 280 × 3.0	134.0	10.50	0	0	2	0.165	0.330	280	1148.14	0.0174
134		E134	140 × 280 × 3.0	134.0	10.50	0	0	3	0.165	0.495	280	1599.29	0.0193
135	G7	E135	70 × 158 × 2.0	66.0	15.00	0	0	1	0.165	0.165	158	294.62	0.0187
136		E136	70 × 158 × 2.0	66.0	15.00	0	0	2	0.165	0.330	158	518.80	0.0218
137		E137	100 × 225 × 3.0	94.0	15.00	0	0	1	0.165	0.165	225	434.67	0.0174
138		E138	100 × 225 × 3.0	94.0	15.00	0	0	2	0.165	0.330	225	750.63	0.0197
139		E139	150 × 338 × 3.0	144.0	15.00	0	0	1	0.165	0.165	338	679.42	0.0156
140		E140	150 × 338 × 3.0	144.0	15.00	0	0	2	0.165	0.335	338	1178.64	0.0180
141		E141	70 × 158 × 2.0	66.0	35.00	0	0	1	0.165	0.165	158	301.04	0.0182
142		E142	70 × 158 × 2.0	66.0	35.00	0	0	2	0.165	0.330	158	515.09	0.0211
143		E143	100 × 225 × 3.0	94.0	35.00	0	0	1	0.165	0.165	225	495.83	0.0164
144		E144	100 × 225 × 3.0	94.0	35.00	0	0	2	0.165	0.330	225	802.39	0.0185

(Continued on following page)

TABLE 2 (*Continued*) Summary of confined concrete filled PVC tube with CFRP.

S.No	Group code	Code	Size: D x H x t	D_c	f_c'	Reinforcement		CFRP			CFRP-depth	P_{FF}	ε_{FF}
			(mm) x (mm)	mm	MPa	Longitudinal	Hoop	No. Of layers	Thickness/ Layers mm	Total thickness mm	mm	kN	mm/ mm
145	G8(P1)	E145	160 × 500 × 2.3	155.4	31.30	10Ø110	6Ø104	1	0.165	0.165	500	1260.62	0.0168
146		E146	160 × 500 × 2.3	155.4	31.30	10Ø110	6Ø104	1	0.165	0.165	20	999.39	0.0150
147		E147	160 × 500 × 2.3	155.4	31.30	10Ø110	6Ø104	1	0.165	0.165	20	917.70	0.0149
148		E148	160 × 500 × 2.3	155.4	31.30	10Ø110	6Ø104	1	0.165	0.165	20	869.74	0.0148
149		E149	160 × 500 × 2.3	155.4	31.30	10Ø110	6Ø104	1	0.165	0.165	20	820.04	0.0147
150		E150	160 × 500 × 2.3	155.4	31.30	10Ø110	6Ø104	2	0.165	0.330	500	1781.51	0.0179
151		E151	160 × 500 × 2.3	155.4	31.30	10Ø110	6Ø104	2	0.165	0.330	20	1227.56	0.0147
152		E152	160 × 500 × 2.3	155.4	31.30	10Ø110	6Ø104	2	0.165	0.330	20	1055.10	0.0140
153		E153	160 × 500 × 2.3	155.4	31.30	10Ø110	6Ø104	2	0.165	0.330	20	962.25	0.0142
154		E154	160 × 500 × 2.3	155.4	31.30	10Ø110	6Ø104	2	0.165	0.330	20	866.80	0.0140
155		E155	160 × 500 × 2.3	155.4	31.30	10Ø110	6Ø104	3	0.165	0.330	500	2361.59	0.0198
156		E156	160 × 500 × 2.3	155.4	31.30	10Ø110	6Ø104	3	0.165	0.330	20	1466.44	0.0147
157		E157	160 × 500 × 2.3	155.4	31.30	10Ø110	6Ø104	3	0.165	0.330	20	1177.14	0.0134
158		E158	160 × 500 × 2.3	155.4	31.30	10Ø110	6Ø104	3	0.165	0.330	20	1036.67	0.0136
159		E159	160 × 500 × 2.3	155.4	31.30	10Ø110	6Ø104	3	0.165	0.330	20	889.18	0.0134
160	G8(P2)	E160	160 × 500 × 3.7	152.6	31.30	10Ø110	6Ø104	1	0.165	0.165	500	1291.10	0.0172
161		E161	160 × 500 × 3.7	152.6	31.30	10Ø110	6Ø104	1	0.165	0.165	20	1033.32	0.0153
162		E162	160 × 500 × 3.7	152.6	31.30	10Ø110	6Ø104	1	0.165	0.165	20	948.52	0.0147
163		E163	160 × 500 × 3.7	152.6	31.30	10Ø110	6Ø104	1	0.165	0.165	20	903.12	0.0147
164		E164	160 × 500 × 3.7	152.6	31.30	10Ø110	6Ø104	1	0.165	0.165	20	852.79	0.0149
165		E165	160 × 500 × 3.7	152.6	31.30	10Ø110	6Ø104	2	0.165	0.330	500	1815.24	0.0185
166		E166	160 × 500 × 3.7	152.6	31.30	10Ø110	6Ø104	2	0.165	0.330	20	1267.86	0.0149
167		E167	160 × 500 × 3.7	152.6	31.30	10Ø110	6Ø104	2	0.165	0.330	20	1088.55	0.0139
168		E168	160 × 500 × 3.7	152.6	31.30	10Ø110	6Ø104	2	0.165	0.330	20	1000.45	0.0145
169		E169	160 × 500 × 3.7	152.6	31.30	10Ø110	6Ø104	2	0.165	0.330	20	905.53	0.0144
170		E170		152.6	31.30	10Ø110	6Ø104	3	0.165	0.330	500	2366.55	0.0199

(Continued on following page)

TABLE 2 (*Continued*) Summary of confined concrete filled PVC tube with CFRP.

S.No	Group code	Code	Size: D x H x t	D_c	f_c'	Reinforcement		CFRP			CFRP-depth	P_{FF}	ε_{FF}
			(mm) x (mm)	mm	MPa	Longitudinal	Hoop	No. Of layers	Thickness/ Layers mm	Total thickness mm	mm	kN	mm/ mm
			160 × 500 × 3.7										
171		E171	160 × 500 × 3.7	152.6	31.30	10Ø110	6Ø104	3	0.165	0.330	20	1498.90	0.0147
172		E172	160 × 500 × 3.7	152.6	31.30	10Ø110	6Ø104	3	0.165	0.330	20	1219.37	0.0133
173		E173	160 × 500 × 3.7	152.6	31.30	10Ø110	6Ø104	3	0.165	0.330	20	1082.60	0.0138
174		E174	160 × 500 × 3.7	152.6	31.30	10Ø110	6Ø104	3	0.165	0.330	20	935.89	0.0137
175	G8(P3)	E175	160 × 500 × 5.4	149.2	31.30	10Ø110	6Ø104	1	0.165	0.165	500	1316.28	0.0174
176		E176	160 × 500 × 5.4	149.2	31.30	10Ø110	6Ø104	1	0.165	0.165	20	1068.28	0.0150
177		E177	160 × 500 × 5.4	149.2	31.30	10Ø110	6Ø104	1	0.165	0.165	20	987.20	0.0150
178		E178	160 × 500 × 5.4	149.2	31.30	10Ø110	6Ø104	1	0.165	0.165	20	942.92	0.0150
179		E179	160 × 500 × 5.4	149.2	31.30	10Ø110	6Ø104	1	0.165	0.165	20	893.81	0.0150
180		E180	160 × 500 × 5.4	149.2	31.30	10Ø110	6Ø104	2	0.165	0.330	500	1832.25	0.0187
181		E181	160 × 500 × 5.4	149.2	31.30	10Ø110	6Ø104	2	0.165	0.330	20	1303.90	0.0149
182		E182	160 × 500 × 5.4	149.2	31.30	10Ø110	6Ø104	2	0.165	0.330	20	1131.63	0.0142
183		E183	160 × 500 × 5.4	149.2	31.30	10Ø110	6Ø104	2	0.165	0.330	20	1042.18	0.0143
184		E184	160 × 500 × 5.4	149.2	31.30	10Ø110	6Ø104	2	0.165	0.330	20	952.23	0.0143
185		E185	160 × 500 × 5.4	149.2	31.30	10Ø110	6Ø104	3	0.165	0.495	500	2405.21	0.0206
186		E186	160 × 500 × 5.4	149.2	31.30	10Ø110	6Ø104	3	0.165	0.495	20	1550.67	0.0150
187		E187	160 × 500 × 5.4	149.2	31.30	10Ø110	6Ø104	3	0.165	0.495	20	1260.47	0.0133
188		E188	160 × 500 × 5.4	149.2	31.30	10Ø110	6Ø104	3	0.165	0.495	20	1133.50	0.0140
189		E189	160 × 500 × 5.4	149.2	31.30	10Ø110	6Ø104	3	0.165	0.495	20	989.83	0.0137
190	G8(P4)	E190	160 × 1000 × 2.3	155.4	36.40	10Ø120	6Ø114	1	0.165	0.165	20	1009.45	0.0168
191		E191	160 × 1000 × 2.3	155.4	36.40	10Ø120	6Ø114	1	0.165	0.165	20	922.30	0.0166
192		E192	160 × 1000 × 2.3	155.4	36.40	10Ø120	6Ø114	1	0.165	0.165	20	872.36	0.0152
193		E193	160 × 1000 × 2.3	155.4	36.40	10Ø120	6Ø114	1	0.165	0.165	20	813.17	0.0188
194		E194	160 × 1000 × 2.3	155.4	36.40	10Ø120	6Ø114	2	0.165	0.330	20	1257.69	0.0172

(Continued on following page)

TABLE 2 (*Continued*) Summary of confined concrete filled PVC tube with CFRP.

S.No	Group code	Code	Size: D x H x t	D_c	f_c'	Reinforcement		CFRP			CFRP-depth	P_{FF}	ε_{FF}
			(mm) x (mm)	mm	MPa	Longitudinal	Hoop	No. Of layers	Thickness/ Layers mm	Total thickness mm	mm	kN	mm/ mm
195		E195	160 × 1000 × 2.3	155.4	36.40	10Ø120	6Ø114	2	0.165	0.330	20	1062.86	0.0159
196		E196	160 × 1000 × 2.3	155.4	36.40	10Ø120	6Ø114	2	0.165	0.330	20	960.76	0.0153
197		E197	160 × 1000 × 2.3	155.4	36.40	10Ø120	6Ø114	2	0.165	0.330	20	852.02	0.0215
198		E198	160 × 1000 × 2.3	155.4	36.40	10Ø120	6Ø114	3	0.165	0.495	20	1492.94	0.0174
199		E199	160 × 1000 × 2.3	155.4	36.40	10Ø120	6Ø114	3	0.165	0.495	20	1189.96	0.0152
200		E200	160 × 1000 × 2.3	155.4	36.40	10Ø120	6Ø114	3	0.165	0.495	20	1036.38	0.0144
201		E201	160 × 1000 × 2.3	155.4	36.40	10Ø120	6Ø114	3	0.165	0.495	20	873.30	0.0203
202	G8(P5)	E202	160 × 1000 × 3.7	152.6	36.40	10Ø120	6Ø114	1	0.165	0.165	20	1045.74	0.0174
203		E203	160 × 1000 × 3.7	152.6	36.40	10Ø120	6Ø114	1	0.165	0.165	20	954.36	0.0167
204		E204	160 × 1000 × 3.7	152.6	36.40	10Ø120	6Ø114	1	0.165	0.165	20	904.99	0.0154
205		E205	160 × 1000 × 3.7	152.6	36.40	10Ø120	6Ø114	1	0.165	0.165	20	846.41	0.0189
206		E206	160 × 1000 × 3.7	152.6	36.40	10Ø120	6Ø114	2	0.165	0.330	20	1289.68	0.0169
207		E207	160 × 1000 × 3.7	152.6	36.40	10Ø120	6Ø114	2	0.165	0.330	20	1100.60	0.0157
208		E208	160 × 1000 × 3.7	152.6	36.40	10Ø120	6Ø114	2	0.165	0.330	20	998.97	0.0153
209		E209	160 × 1000 × 3.7	152.6	36.40	10Ø120	6Ø114	2	0.165	0.330	20	888.53	0.0214
210		E210	160 × 1000 × 3.7	152.6	36.40	10Ø120	6Ø114	3	0.165	0.495	20	1537.37	0.0175
211		E211	160 × 1000 × 3.7	152.6	36.40	10Ø120	6Ø114	3	0.165	0.495	20	1234.17	0.0151
212		E212	160 × 1000 × 3.7	152.6	36.40	10Ø120	6Ø114	3	0.165	0.495	20	1081.43	0.0144
213		E213	160 × 1000 × 3.7	152.6	36.40	10Ø120	6Ø114	3	0.165	0.495	20	913.26	0.0209
214	G8(P6)	E214	160 × 1000 × 5.4	149.2	36.40	10Ø120	6Ø114	1	0.165	0.165	20	1084.09	0.0169
215		E215	160 × 1000 × 5.4	149.2	36.40	10Ø120	6Ø114	1	0.165	0.165	20	993.64	0.0167
216		E216	160 × 1000 × 5.4	149.2	36.40	10Ø120	6Ø114	1	0.165	0.165	20	944.34	0.0159
217		E217	160 × 1000 × 5.4	149.2	36.40	10Ø120	6Ø114	1	0.165	0.165	20	884.89	0.0194
218		E218	160 × 1000 × 5.4	149.2	36.40	10Ø120	6Ø114	2	0.165	0.330	20	1324.90	0.0166
219		E219	160 × 1000 × 5.4	149.2	36.40	10Ø120	6Ø114	2	0.165	0.330	20	1138.51	0.0151

(Continued on following page)

TABLE 2 (*Continued*) Summary of confined concrete filled PVC tube with CFRP.

S.No	Group code	Code	Size: D x H x t	D_c	f_c'	Reinforcement		CFRP			CFRP-depth	P_{FF}	ε_{FF}
			(mm) x (mm)	mm	MPa	Longitudinal	Hoop	No. Of layers	Thickness/ Layers mm	Total thickness mm	mm	kN	mm/mm
220		E220	160 × 1000 × 5.4	149.2	36.40	10Ø120	6Ø114	2	0.165	0.330	20	1043.25	0.0153
221		E221	160 × 1000 × 5.4	149.2	36.40	10Ø120	6Ø114	2	0.165	0.330	20	928.59	0.0211
222		E222	160 × 1000 × 5.4	149.2	36.40	10Ø120	6Ø114	3	0.165	0.495	20	1572.69	0.0173
223		E223	160 × 1000 × 5.4	149.2	36.40	10Ø120	6Ø114	3	0.165	0.495	20	1280.92	0.0150
224		E224	160 × 1000 × 5.4	149.2	36.40	10Ø120	6Ø114	3	0.165	0.495	20	1130.97	0.0145
225		E225	160 × 1000 × 5.4	149.2	36.40	10Ø120	6Ø114	3	0.165	0.495	20	960.03	0.0204
226	G9(P1)	E226	200 × 500 × 7.8	184.4	28.50	10Ø200	8Ø194	1	0.165	0.165	20	1497.35	0.0163
227		E227	200 × 500 × 7.8	184.4	28.50	10Ø200	8Ø194	1	0.165	0.165	20	1441.09	0.0161
228		E228	200 × 500 × 7.8	184.4	28.50	10Ø200	8Ø194	1	0.165	0.165	20	1394.81	0.0157
229		E229	200 × 500 × 7.8	184.4	28.50	10Ø200	8Ø194	1	0.165	0.165	20	1366.71	0.0167
230		E230	200 × 500 × 7.8	184.4	28.50	10Ø200	8Ø194	1	0.165	0.165	20	1346.28	0.0157
231		E231	200 × 500 × 7.8	184.4	28.50	10Ø200	8Ø194	1	0.165	0.165	20	1307.27	0.0168
232		E232	200 × 500 × 7.8	184.4	28.50	10Ø200	8Ø194	2	0.165	0.330	20	1774.40	0.0163
233		E233	200 × 500 × 7.8	184.4	28.50	10Ø200	8Ø194	2	0.165	0.330	20	1664.99	0.0160
234		E234	200 × 500 × 7.8	184.4	28.50	10Ø200	8Ø194	2	0.165	0.330	20	1587.15	0.0160
235		E235	200 × 500 × 7.8	184.4	28.50	10Ø200	8Ø194	2	0.165	0.330	20	1519.68	0.0179
236		E236	200 × 500 × 7.8	184.4	28.50	10Ø200	8Ø194	2	0.165	0.330	20	1480.47	0.0155
237		E237	200 × 500 × 7.8	184.4	28.50	10Ø200	8Ø194	2	0.165	0.330	20	1392.94	0.0159
238		E238	200 × 500 × 7.8	184.4	28.50	10Ø200	8Ø194	3	0.165	0.495	20	2070.22	0.0168
239		E239	200 × 500 × 7.8	184.4	28.50	10Ø200	8Ø194	3	0.165	0.495	20	1903.55	0.0165
240		E240	200 × 500 × 7.8	184.4	28.50	10Ø200	8Ø194	3	0.165	0.495	20	1782.42	0.0163
241		E241	200 × 500 × 7.8	184.4	28.50	10Ø200	8Ø194	3	0.165	0.495	20	1679.68	0.0195
242		E242	200 × 500 × 7.8	184.4	28.50	10Ø200	8Ø194	3	0.165	0.495	20	1617.72	0.0158
243		E243	200 × 500 × 7.8	184.4	28.50	10Ø200	8Ø194	3	0.165	0.495	20	1473.21	0.0157
244	E9(P2)	E244	200 × 500 × 7.8	184.4	45.00	10Ø200	8Ø194	1	0.165	0.165	20	1793.85	0.0159

(Continued on following page)

TABLE 2 (*Continued*) Summary of confined concrete filled PVC tube with CFRP.

S.No	Group code	Code	Size: D x H x t	D_c	f_c'	Reinforcement		CFRP			CFRP-depth	P_{FF}	ε_{FF}
			(mm) x (mm)	mm	MPa	Longitudinal	Hoop	No. Of layers	Thickness/ Layers mm	Total thickness mm	mm	kN	mm/mm
245		E245	200 × 500 × 7.8	184.4	45.00	10Ø200	8Ø194	1	0.165	0.165	20	1739.75	0.0159
246		E246	200 × 500 × 7.8	184.4	45.00	10Ø200	8Ø194	1	0.165	0.165	20	1703.04	0.0155
247		E247	200 × 500 × 7.8	184.4	45.00	10Ø200	8Ø194	1	0.165	0.165	20	1675.39	0.0159
248		E248	200 × 500 × 7.8	184.4	45.00	10Ø200	8Ø194	1	0.165	0.165	20	1655.70	0.0155
249		E249	200 × 500 × 7.8	184.4	45.00	10Ø200	8Ø194	1	0.165	0.165	20	1607.17	0.0156
250		E250	200 × 500 × 7.8	184.4	45.00	10Ø200	8Ø194	2	0.165	0.330	20	2063.35	0.0163
251		E251	200 × 500 × 7.8	184.4	45.00	10Ø200	8Ø194	2	0.165	0.330	20	1956.43	0.0163
252		E252	200 × 500 × 7.8	184.4	45.00	10Ø200	8Ø194	2	0.165	0.330	20	1876.56	0.0159
253		E253	200 × 500 × 7.8	184.4	45.00	10Ø200	8Ø194	2	0.165	0.330	20	1817.21	0.0173
254		E254	200 × 500 × 7.8	184.4	45.00	10Ø200	8Ø194	2	0.165	0.330	20	1782.72	0.0159
255		E255	200 × 500 × 7.8	184.4	45.00	10Ø200	8Ø194	2	0.165	0.330	20	1688.75	0.0154
256		E256	200 × 500 × 7.8	184.4	45.00	10Ø200	8Ø194	3	0.165	0.495	20	2339.82	0.0167
257		E257	200 × 500 × 7.8	184.4	45.00	10Ø200	8Ø194	3	0.165	0.495	20	2164.47	0.0162
258		E258	200 × 500 × 7.8	184.4	45.00	10Ø200	8Ø194	3	0.165	0.495	20	2053.09	0.0162
259		E259	200 × 500 × 7.8	184.4	45.00	10Ø200	8Ø194	3	0.165	0.495	20	1960.78	0.0187
260		E260	200 × 500 × 7.8	184.4	45.00	10Ø200	8Ø194	3	0.165	0.495	20	1904.14	0.0158
261		E261	200 × 500 × 7.8	184.4	45.00	10Ø200	8Ø194	3	0.165	0.495	20	1764.36	0.0159
262	G10(P1)	E262	165 × 495 × 4.0	157.0	33.60	0	0	1	0.165	0.165	495	1108.62	0.0160
263		E263	165 × 495 × 4.0	157.0	33.60	0	0	1	0.165	0.165	15	732.06	0.0153
264		E264	165 × 495 × 4.0	157.0	33.60	0	0	1	0.165	0.165	15	702.11	0.0162
265		E265	165 × 495 × 4.0	157.0	33.60	0	0	1	0.165	0.165	15	671.22	0.0162
266		E266	165 × 495 × 4.0	157.0	33.60	0	0	1	0.165	0.165	15	654.61	0.0162
267		E267	165 × 495 × 4.0	157.0	33.60	0	0	1	0.165	0.165	15	643.73	0.0145
268		E268	165 × 495 × 4.0	157.0	33.60	0	0	2	0.165	0.330	495	1608.02	0.0163
269		E269	165 × 495 × 4.0	157.0	33.60	0	0	2	0.165	0.330	15	836.75	0.0173
270		E270		157.0	33.60	0	0	2	0.165	0.330	15	781.44	0.0170

(Continued on following page)

TABLE 2 (*Continued*) Summary of confined concrete filled PVC tube with CFRP.

S.No	Group code	Code	Size: D x H x t	D_c	f_c'	Reinforcement		CFRP			CFRP-depth	P_{FF}	ε_{FF}
			(mm) x (mm)	mm	MPa	Longitudinal	Hoop	No. Of layers	Thickness/ Layers mm	Total thickness mm	mm	kN	mm/mm
			165 × 495 × 4.0										
271		E271	165 × 495 × 4.0	157.0	33.60	0	0	2	0.165	0.330	15	723.19	0.0170
272		E272	165 × 495 × 4.0	157.0	33.60	0	0	2	0.165	0.330	15	685.93	0.0180
273		E273	165 × 495 × 4.0	157.0	33.60	0	0	2	0.165	0.330	15	656.65	0.0155
274		E274	165 × 495 × 4.0	157.0	33.60	0	0	3	0.165	0.495	495	2012.64	0.0159
275		E275	165 × 495 × 4.0	157.0	33.60	0	0	3	0.165	0.495	15	942.48	0.0189
276		E276	165 × 495 × 4.0	157.0	33.60	0	0	3	0.165	0.495	15	856.09	0.0180
277		E277	165 × 495 × 4.0	157.0	33.60	0	0	3	0.165	0.495	15	769.38	0.0178
278		E278	165 × 495 × 4.0	157.0	33.60	0	0	3	0.165	0.495	15	714.95	0.0194
279		E279	165 × 495 × 4.0	157.0	33.60	0	0	3	0.165	0.495	15	669.64	0.0157
280	G10(P2)	E280	165 × 495 × 4.0	157.0	67.20	0	0	1	0.165	0.165	495	1366.85	0.0161
281		E281	165 × 495 × 4.0	157.0	67.20	0	0	1	0.165	0.165	15	1061.35	0.0154
282		E282	165 × 495 × 4.0	157.0	67.20	0	0	1	0.165	0.165	15	1035.11	0.0157
283		E283	165 × 495 × 4.0	157.0	67.20	0	0	1	0.165	0.165	15	1002.38	0.0158
284		E284	165 × 495 × 4.0	157.0	67.20	0	0	1	0.165	0.165	15	981.08	0.0163
285		E285	165 × 495 × 4.0	157.0	67.20	0	0	2	0.165	0.330	495	1829.00	0.0161
286		E286	165 × 495 × 4.0	157.0	67.20	0	0	2	0.165	0.330	15	1138.00	0.0169
287		E287	165 × 495 × 4.0	157.0	67.20	0	0	2	0.165	0.330	15	1096.07	0.0165
288		E288	165 × 495 × 4.0	157.0	67.20	0	0	2	0.165	0.330	15	1038.84	0.0167
289		E289	165 × 495 × 4.0	157.0	67.20	0	0	2	0.165	0.330	15	999.96	0.0176
290		E290	165 × 495 × 4.0	157.0	67.20	0	0	3	0.165	0.495	495	2270.81	0.0161
291		E291	165 × 495 × 4.0	157.0	67.20	0	0	3	0.165	0.495	15	1216.70	0.0175
292		E292	165 × 495 × 4.0	157.0	67.20	0	0	3	0.165	0.495	15	1149.33	0.0174
293		E293	165 × 495 × 4.0	157.0	67.20	0	0	3	0.165	0.495	15	1065.96	0.0177
294		E294	165 × 495 × 4.0	157.0	67.20	0	0	3	0.165	0.495	15	1011.50	0.0190
295	G11	E295	160 × 750 × 2.3	155.4	31.30	10Ø120	6Ø114	1	0.165	0.165	750	1242.21	0.0169

(Continued on following page)

TABLE 2 (*Continued*) Summary of confined concrete filled PVC tube with CFRP.

S.No	Group code	Code	Size: D x H x t	D_c	f_c'	Reinforcement		CFRP			CFRP-depth	P_{FF}	ε_{FF}
			(mm) x (mm)	mm	MPa	Longitudinal	Hoop	No. Of layers	Thickness/ Layers mm	Total thickness mm	mm	kN	mm/ mm
296		E296	160 × 750 × 3.7	152.6	31.30	10Ø120	6Ø114	1	0.165	0.165	750	1274.24	0.0176
297		E297	160 × 750 × 5.4	149.2	31.30	10Ø120	6Ø114	1	0.165	0.165	750	1304.98	0.0178
298		E298	160 × 750 × 2.3	155.4	31.30	10Ø120	6Ø114	3	0.165	0.495	750	2331.86	0.0192
299		E299	160 × 750 × 3.7	152.6	31.30	10Ø120	6Ø114	3	0.165	0.495	750	2310.14	0.0193
300		E300	160 × 750 × 5.4	149.2	31.30	10Ø120	6Ø114	3	0.165	0.495	750	2330.70	0.0197
301	G12	E301	160 × 1000 × 2.3	155.4	31.30	10Ø120	6Ø114	2	0.165	0.330	20	1740.13	0.0174
302		E302	160 × 1000 × 3.7	152.6	31.30	10Ø120	6Ø114	2	0.165	0.330	20	1771.88	0.0177
303		E303	160 × 1000 × 5.4	149.2	31.30	10Ø120	6Ø114	2	0.165	0.330	20	1790.43	0.0180
304		E304	160 × 1000 × 2.3	155.4	31.30	10Ø120	6Ø114	2	0.165	0.330	20	1196.84	0.0167
305		E305	160 × 1000 × 3.7	152.6	31.30	10Ø120	6Ø114	2	0.165	0.330	20	1256.44	0.0175
306		E306	160 × 1000 × 5.4	149.2	31.30	10Ø120	6Ø114	2	0.165	0.330	20	1265.09	0.0168
307		E307	160 × 1000 × 2.3	155.4	31.30	10Ø120	6Ø114	2	0.165	0.330	20	1007.96	0.0153
308		E308	160 × 1000 × 3.7	152.6	31.30	10Ø120	6Ø114	2	0.165	0.330	20	1067.89	0.0161
309		E309	160 × 1000 × 5.4	149.2	31.30	10Ø120	6Ø114	2	0.165	0.330	20	1092.08	0.0156
310		E310	160 × 1000 × 2.3	155.4	31.30	10Ø120	6Ø114	2	0.165	0.330	20	907.52	0.0149
311		E311	160 × 1000 × 3.7	152.6	31.30	10Ø120	6Ø114	2	0.165	0.330	20	967.21	0.0156
312		E312	160 × 1000 × 5.4	149.2	31.30	10Ø120	6Ø114	2	0.165	0.330	20	996.59	0.0149

D: Diameter of circular section (mm), H: Height of specimen (mm), D_c: Diameter of the concrete core without PVC, tube (mm), f_c': strength of unconfined concrete cylinder under compression (MPa), ε_{FF}: Failure finite element modeling strain (mm/mm), P_{FF}: Failure finite element modeling Load (kN), CFRP, Carbon Fibre Reinforced Polymer.

3.2 Material models

3.2.1 Confined concrete

The concrete core is confined by the PVC tube. Hence, it was modeled as a confined concrete. Under load, concrete transit from the elastic stage to the plastic stage and then fails. In the elastic region, the constitutive model of the concrete was expressed by its elastic modulus, E_c and Poisson's ratio v. Mostly, Poisson's ratio of 0.2 is set for concrete. The elastic modulus of the concrete was deduced from Eq. 1 as recommended by (ACI Standards, 2019).

$$E_c = 4700\sqrt{f_c'} \quad (1)$$

Where f_c' is the cylinder compressive strength of concrete

Beyond the elastic limit, transitions of concrete to the plastic region begins, which makes interaction between concrete and PVC tubes starts. At this stage, there exist interactions and contact pressure between the PVC tube's inner surface and the outer surface of the concrete due to the plastic expansion of the concrete. In this case, a confined peak strain model Concrete Damage Plasticity Model (CDPM) in ABAQUS was used to simulate the concrete core (Raza et al., 2019; Ozkilic et al.,

2021a). CDPM utilizes the two main failure criteria *viz.*, tensile cracking and compressive crushing (Ozkilic et al., 2021b; Ozkilic et al., 2021c). The constitutive relations of the concrete were expressed by plastic flow potential, yield surface function, and softening rule/strain hardening. The plastic flow potential was expressed by the dilation angle (ψ) and flow potential eccentricity (e), while the ratio of biaxial compressive strength to the uniaxial compressive strength of concrete (f_{bo}/f_c') and the ratio of tensile meridian second stress invariant to the compression meridian (K_c) denotes the yield surface function. However, the confinement of the concrete core by the PVC tube was defined with the confinement factor, $\xi_c = f_{PVC}A_{PVC}/f_c'A_c$. The parameters are presented in Table 3. Stress and strain for the concrete used for this investigation are shown in Figure 1.

At the onset of loading, the constraint of the PVC tube on the concrete core was not considered, therefore, the stress state of the concrete core is comparable to the unconfined concrete. Therefore, Eq. 2 (Papanikolaou and Kappos, 2007) was used to describe the ascending stress-strain response curve till the peak stress. The strain of the confined concrete at peak first peak load (ε_{cc1}) is derived from Eq. 3. In this study numerical simulation, the elastic stress response equates to 45%–50% of the maximum concrete cylinder strength for confined and unconfined concrete.

$$\sigma_c = \frac{2f_c'\left(\frac{\varepsilon_c}{\varepsilon_{cc1}}\right)}{1+\left(\frac{\varepsilon_c}{\varepsilon_{cc1}}\right)^2} \tag{2}$$

$$\left[\frac{\varepsilon_{cc1}}{\varepsilon_c}\right] = 0.808\left[\frac{H}{D}\right]^{0.5}\left\{1+6.241\left[\frac{f_{ls}}{f_c'}\right]^{0.85}+15.223\left[\frac{f_{lpvc}}{f_c'}\right]^{0.99}\right\} \tag{3}$$

Upon reaching the peak stress, the response curve became a plateau, which indicated the onset of the development of the plastic response stage. The plateau proceeded and the concrete core expands laterally. The lateral expansion was resisted by the PVC tube. The model proposed by Isleem et al. (2022) through multi-linear regression analysis was used to describe the strain of the confined concrete core.

3.2.2 PVC

The stress-strain response and softening rule of PVC plastic would be different from that of concrete. PVC plastic is a ductile material with large strain. It is regarded as an isotropic material due to its similar properties in all directions. The PVC tube is modeled as a von mises material with isotropic hardening. For the effective modeling of the material, it is imperative to define the parameters of yield strength, Poisson ratio, elastic modulus, and inelastic strain for the elastic and plastic material definition. As reported, the test data of PVC employed are presented in Table 4; Figure 2.

3.2.3 Steel material

Steel is used for the end plates and reinforcement bars. The density of hoop and longitudinal steel used in this investigation is 7850 kg/m^3. Young's modulus of steel is 2×10^5 N/mm^2 and Poisson's ratio of 0.20 is used for this investigation at the elastic stage. Whereas at the plastic stage of steel, the yield stress of steel is 500 N/mm^2 and the plastic strain is zero. Reinforcement is embedded in the whole model with fractional exterior tolerance of 0.05.

3.2.4 Carbon fiber reinforced polymer

CFRP is viewed as an orthotropic material frequently. High tensile strength is noted, in the longitudinal direction and displays an elastic behavior, but the compressive strength of CFRP is almost neglected. Therefore, the CFRP properties are specified using the "LAMINA" material type. The failure mode of CFRP was the tensile fracture, so the damage behavior of CFRP must be considered. The tensile failure stress of CFRP is considered as 3612 MPa and the corresponding tensile failure strain is 0.016125 is used for this analytical investigation. Similar tensile failure stress and young's modulus were reported by Xu et al. (2021). CFRP was chosen as the wrapped material partially/fully, with a different number of layers of the CFPT columns. The mass density of CFRP used in this investigation is 1.7×10^{-9} kg/m^3 and the thickness of each layer is 20 mm. The properties of CFRP used in this investigation are tabulated in Table 5.

3.3 Boundary conditions and types of loadings

All degrees of freedom on the bottom of the columns in models are constrained. Concentric load is applied on the top of the columns along the main axis of the column under displacement mode. Boundary conditions on the top surfaces with displacement on the X-axis and Y-axis are zero. On the top of the column specimen, the displacement along the main axis is allowed only. Whereas rotation along all three axes is set to be free. For the bottom surface, the displacement and rotation are arrested on all three axes.

3.4 Meshing

The sweep technique creates a three-dimensional mesh by moving a two-dimensional mesh along a sweep path (3DS., 2014). Elements of 10 mm in size and the Sweep technique have been used for the concrete core. Elements of 15 mm and 20 mm in size and the Sweep Technique have been used for PVC pipe in columns with and without gaps at two ends, respectively. Figure 3 shows the finite element modeling for CFPT tubes.

4 Model validation

4.1 Failure modes

The comparison of the experimental data and numerical results presents the accuracy and precision of the finite element model for

TABLE 3 Concrete damaged plasticity parameters.

Ψ	Kc	e	fbo/fc'	μ
35°	0.667	0.1	1.16	0.0002

validation. Figure 4 presents the comparison of the test results and numerical simulations. It can be observed that there is a correlation in the failure mode.

4.2 Discussions of experimental and model results

In the literature, it is noted that the results provided by FE models are higher when compared to that of experimental test value (Isleem et al., 2022). Figure 5 represents the axial strain load curves obtained from experimental testing and FE simulation results for specimens with and without CFRP wrapping on CFPT columns selected from (Guo et al., 2008; Woldemariam et al., 2019; Gupta, 2013; Feng and Ditao, 2013). A comparison of results displayed in Figures 5A–F is selected based on variations in different parameters from different authors of literature. It is also noted that the experimental results and simulation results are having an almost similar pattern for the axial strain-axial load curve and it is also confirmed in the literature (Isleem et al., 2022).

Both CFPT (Figures 5A–C) and CCFPT (Figures 5D–F) show a similar pattern of axial load–strain curve for both experimental and FE results.

5 Test results and discussions

5.1 Failure modes

Two different types of specimens are simulated with and without longitudinal reinforcement. Specimens are wrapped with CFRP at different depths and layers. When a specimen without longitudinal reinforcement is loaded axially, the cracks are initiated at mid-height when the peak load is reached. After peak load carrying capacity was reached, followed by spalling of concrete but it is prevented by CFRP wraps until rupture as shown in Figures 6A–F. Aksoylu et al., 2022 compared the experimental and numerical investigation of load bearing capacity of FRP composites.

The failure mode of unconfined CFPT and CCFPT columns was first initiated with mid-height cracks. On further loading, the maximum load-carrying capacity is reached, followed by concrete spalling and buckling of longitudinal reinforcement as shown in Figures 7A–L. Once bucking of longitudinal reinforcement was reached but buckling of columns is prevented until the eventual rupture of the CFRP wraps. At the mid-height of the specimens, the rupture of the wraps originated around the corners of the column sections. Similar behavior of failure modes is reported in the literature (Wang and Wu., 2008; Abbasnia et al., 2012).

5.2 Axial load–axial strain

Specimens having CFRP wraps leads to an increase in the axial strength but with a very low rate likened to the axial strain.

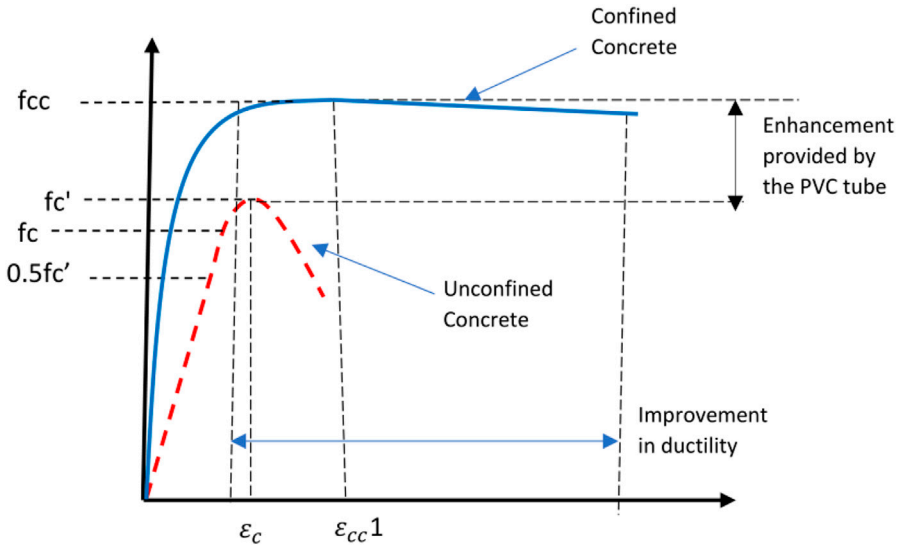

FIGURE 1
Stress-strain curve for unconfined and confined concrete.

TABLE 4 Test data for PVC tube.

Author	Poisson's ratio	Modulus of elasticity (GPa)	Ultimate strength (MPa)	Thickness of the PVC tube (mm)
Woldemariam et al. (2019)	0.339	3.61	50.10	2.50, 3.00
Gupta, (2013)	0.380	3.38	27.5–52.0	3.90, 4.25
Bandyopadhyay et al. (2019)	0.380	3.38	33.16	2.30, 3.70, 5.40
Alatshan et al. (2022)	0.342	2.038	33.4–34.2	2.00, 3.00
Fang et al. (2020)	0.40	3.16	68.0	4.25
Chang et al. (2021)	0.400	4.83	29.01	5.00
Feng and Diato (2013)	0.375	3.15	62.00	3.90
Guo et al. (2008)	0.34	3.68	50.00	7.80

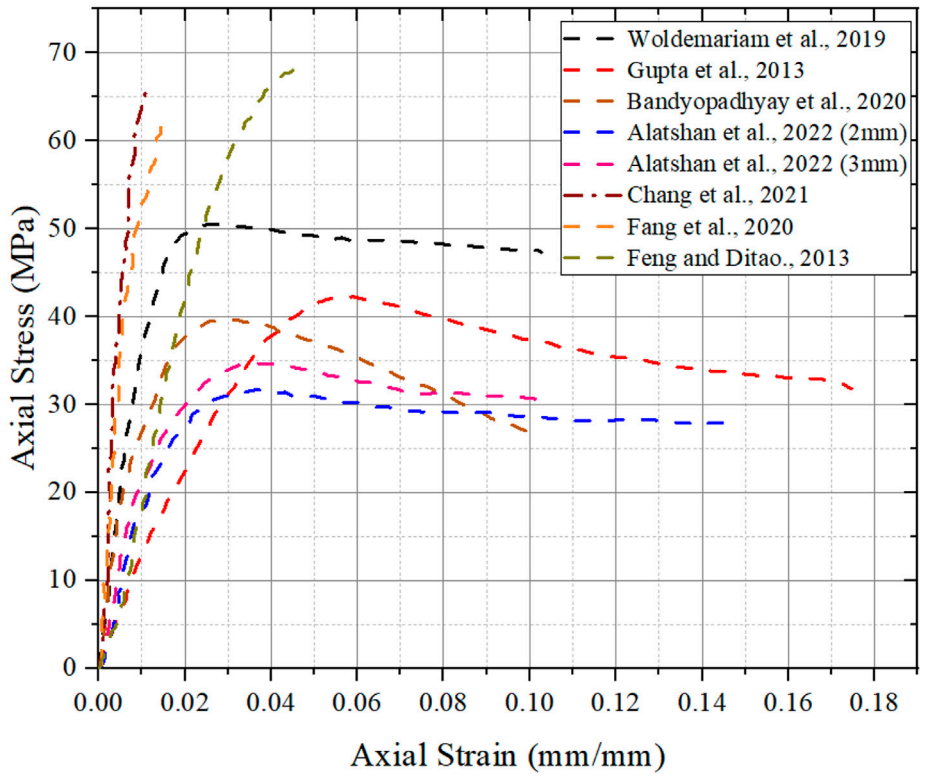

FIGURE 2
Stress-strain response for PVC material used for the present study.

Peak axial strain varied more than thrice that of unconfined concrete and these results are consistent with other results reported in the literature (Hany et al., 2016; Isleem et al., 2018a). Specimens unreinforced by CFRP wrapping experienced gains in the peak strain, whereas there is no observed improvement in their peak strain. Confined specimens displayed a decreased strength due to the low resistance of the CFRP wrap against the dilation and lateral expansion of the core concrete. Stress-strain test results correspond to specimens confined with a similar number of CFRP layers wrapped with different hoop reinforcements showing different behavior. It is also noted that the axial

TABLE 5 Properties of CFRP used in this investigation.

Youngs modulus (MPa)			Poisson's ratio			Shear modulus (MPa)		
E_{12}	E_{13}	E_{23}	μ_{12}	μ_{13}	μ_{23}	G_{12}	G_{13}	G_{23}
224,000	18,581	18,581	0.20	0.20	0.30	12,576	12,576	7147

stress and strain for the reinforced and unreinforced column shows different behavior. Confinement provided by the external CFRP wrapping decreases as the cross-sectional specimen column increases and is also confirmed by Isleem et al. (2018b). An increase in the shear capacity of the reinforced concrete section with CFRP wrapping is reported by Mhanna et al. (2020).

6 Influence of the tested parameters

6.1 Effect of CFRP hoop spacing

The ultimate axial load-carrying capacity increases with the increase in the number of CFRP layers as noted in Figure 8. Additionally, an increase in CFRP hoop spacing results in a decrease in ultimate axial load-carrying capacity. When CFRP thickness increased from 20 mm to 100 mm, the ultimate axial load decreased from 1807.41 kN to 1179.74 kN for 3-layer CFRP, but for 1-layer CFRP, the ultimate axial load decreased from 1214.75 kN to 1016.74 kN is reported from Figure 8A. A decrease in the ultimate axial load is in the range of 1.53, 1.35, and 1.19 times for 3-layer, 2-layer, and 1-layer CFRP from 20mm to 100 mm hoop spacing. From Figure 8B, it is noted that the ultimate axial load decreases in the range of 1.45, 1.32, and 1.17 times for 3-layer, 2-layer, and 1-layer CFRP from 29 mm to 127 mm hoop spacing. Ultimate axial load decreases in the range of 1.87, 1.51, and 1.28 times for the 3-layer, 2-layer and 1-layer CFRP from 20mm to 100 mm hoop spacing for group 3 is noted in Figure 8C.

From Figure 8D, it is noted that the ultimate axial load decreases in the range of 1.81, 1.56, and 1.26 times for 3-layer, 2-layer, and 1-layer CFRP from 20 mm to 100 mm hoop spacing. Ultimate axial load decreases in the range of 3.94, 3.08, and 2.11 times for the 3-layer, 2-layer and 1-layer CFRP from 0mm to 60 mm hoop spacing for group 6 (part 1) is noted in Figure 8E. From Figure 8F, it is noted that the ultimate axial load decreases in the range of 3.80, 2.77, and 1.87 times for 3-layer, 2-layer, and 1-layer CFRP from 0mm to 60 mm hoop spacing. From Figure 8, the following results are summarized:

- The effect of the slenderness ratio is more on the hoop spacing in terms of the ultimate axial load
- The impact of PVC tube thickness is moderate on the hoop spacing in terms of ultimate axial load
- A slight influence of confined concrete strength on the hoop spacing in terms of ultimate axial load

When hoop spacing is increased from 0 mm to 100 mm, an ultimate axial load decrease from 1260.62 kN to 820.04 kN, 1781.51 kN–866.80 kN, and 2361.59 kN–889.18 kN for 1-layer, 2-layer, and 3-layer CFRP is observed from Figure 9A. Decreases in the ultimate axial load for 1-layer, 2-layer, and 3-layer CFRP are in the range of 1.54, 2.05, and 2.65 times for 0 mm when compared to 100 mm hoop spacing. From Figure 9B, it is noted that the decrease in the ultimate axial load for 1-layer, 2-layer, and 3-layer CFRP is in the range of 1.51, 2.01, and 2.53 times for 0 mm when compared to 100 mm hoop spacing.

A decrease in the failure axial load for 1-layer, 2-layer, and 3-layer CFRP is in the range of 1.47, 1.92, and 2.43 times for 0 mm, when compared to 100 mm hoop spacing, is observed in Figure 9C. With an increase in PVC thickness, there is an increase in failure axial load, and also, the rate of reduction of failure axial load to increase in CFRP layers is slow is observed. From Figure 9D, it is noted that the decrease in the failure axial load for 1-layer, 2-layer, and 3-layer CFRP is in the range of 1.24, 1.48, and 1.71 times for 20 mm when compared to 120 mm hoop spacing.

A decrease in the failure axial load for 1-layer, 2-layer, and 3-layer CFRP is in the range of 1.24, 1.45, and 1.68 times for 20 mm, when compared to 120 mm hoop spacing, is observed in Figure 9E. From Figure 9F, it is noted that the decrease in the failure axial load for 1-layer, 2-layer, and 3-layer CFRP is in the range of 1.23, 1.43, and 1.64 times for 20 mm when compared to 120 mm hoop spacing. From Figure 9, the following results are summarized:

- The effect of PVC tube thickness is more on the hoop spacing in terms of failure axial load under all other factors are constant
- The impact of the confined concrete load is moderate on the hoop spacing in terms of failure axial load and all other factors are constant.

The effect of CFRP hoop spacing on the failure axial load for the CCFPT columns with reinforcement is shown in Figure 10. A decrease in the failure axial load for 1-layer, 2-layer, and 3-layer CFRP is in the range of 1.15, 1.27, and 1.41 times for 20 mm, when compared to 100 mm hoop spacing, is observed in

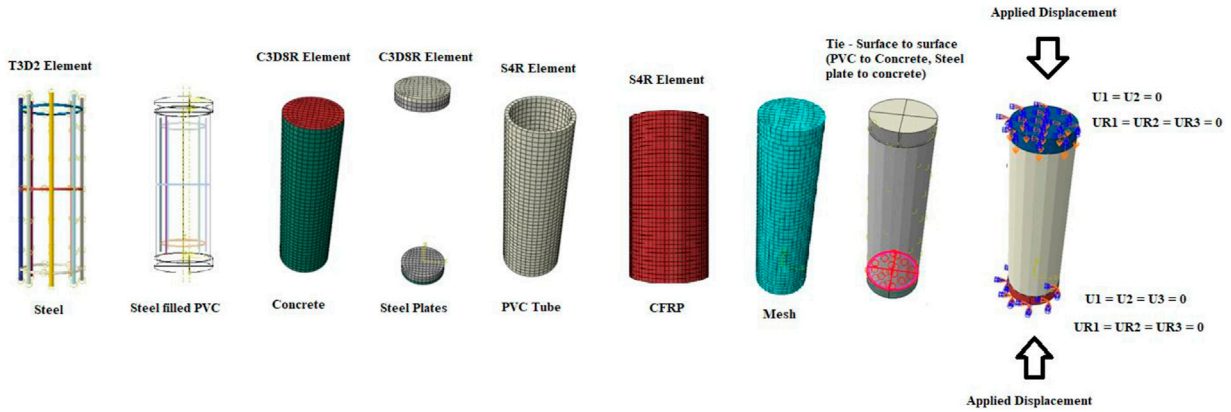

FIGURE 3
Finite element type, loading conditions, boundary conditions, and contact surface.

Figure 10A. From Figure 10B, it is noted that the decrease in the failure axial load for 1-layer, 2-layer, and 3-layer CFRP is in the range of 1.12, 1.22, and 1.33 times for 20 mm when compared to 100 mm hoop spacing. A decrease in the failure axial load for 1-layer, 2-layer, and 3-layer CFRP is in the range of 1.72, 2.45, and 3.01 times for 0 mm, when compared to 105 mm hoop spacing, is observed in Figure 10C. From Figure 10D, it is noted that the decrease in the failure axial load for 1-layer, 2-layer, and 3-layer CFRP is in the range of 1.39, 1.83, and 2.25 times for 0 mm when compared to 80 mm hoop spacing. From Figure 10, the following results are summarized:

- Increase in failure load carrying capacity of a specimen with reinforcement, when confined concrete strength is increased.
- The effect of spacing between main longitudinal bars and hoop bars on the failure load carrying capacity of specimens is noted.

Confinement of CFRP wraps directed to an increase in the axial load but with a very low rate compared to the axial strain is already reported by Isleem et al. (2018a). It is also reported that the addition of CFRP wrapping not only increases the lateral confinement but also the compressive strength and ductility could be improved drastically (Jin et al., 2020). Usage of the optimum amount of CFRP in reinforced concrete structures (Gemi et al., 2022b).

6.2 Effect of CFRP depth

The influence of the overall depth of CFRP on the failure axial load of unreinforced CFPT columns is observed in two different scenarios: 1. CFRP depth is maintained as constant throughout the depth of the specimen (Figure 11A) and 2. CFRP depth is varied throughout the depth of the specimen (Figures 11B, 12A). CFRP depth is kept as constant as 20 mm for group 1 but CFRP hoop spacing is kept as clear to clear distance between CFRP wrapping but it is varied from 20 mm to 100 mm. When the number of layers is increased from 1 to 2 and 3 the failure axial load is increased to 21.86% and 48.79% as compared to layer 1. CFRP hoop spacing is increased as 30 mm, 40 mm, 50 mm, 60 mm, and 100 mm for layer 1, and the failure axial load is increased by 5.63%, 8.54%, and 10.59% when compared to 20 mm CFRP hoop spacing.

Whereas for layer 2, CFRP hoop spacing increased as 30 mm, 40 mm, 50 mm, 60 mm, and 100 mm, the failure axial load increased by 7.07%, 12.92%, 16.43%, 19.71%, and 25.68% compared to 20 mm CFRP hoop spacing. When the number of layers is further increased to layer 3, CFRP hoop spacing is increased as 30 mm, 40 mm, 50 mm, 60 mm, and 100 mm, and failure axial load increased by 11.25%, 18.74%, 23.35%, 27.35%, and 34.73% compared to 20 mm CFRP hoop spacing. From this, it can be concluded, that at constant CFRP depth, with an increase in some layers as layer 3, the increase in failure axial load is higher when compared to layer 1.

CFRP depth is increased from 20 mm to 180 mm, there is an increase in the failure axial load from 202.68 kN to 1016.14 kN for layer 1 is observed. For layer 3, the failure axial load increases from 257.78 kN to 1016.14 kN for group 6 (part 1) for the confined concrete compressive load as 10.5 MPa with CFRP hoop spacing as 20 mm, 60 mm, and 0 mm. An increase in confined concrete compressive strength of 24.12 MPa, there is an increase in failure axial load for group 6 (part 2) is noted. When CFRP wrapping depth is increased there is an increase in failure axial load is noted in Figure 12B. Even though CFRP wrapping depth is kept constant and hoop spacing is increased

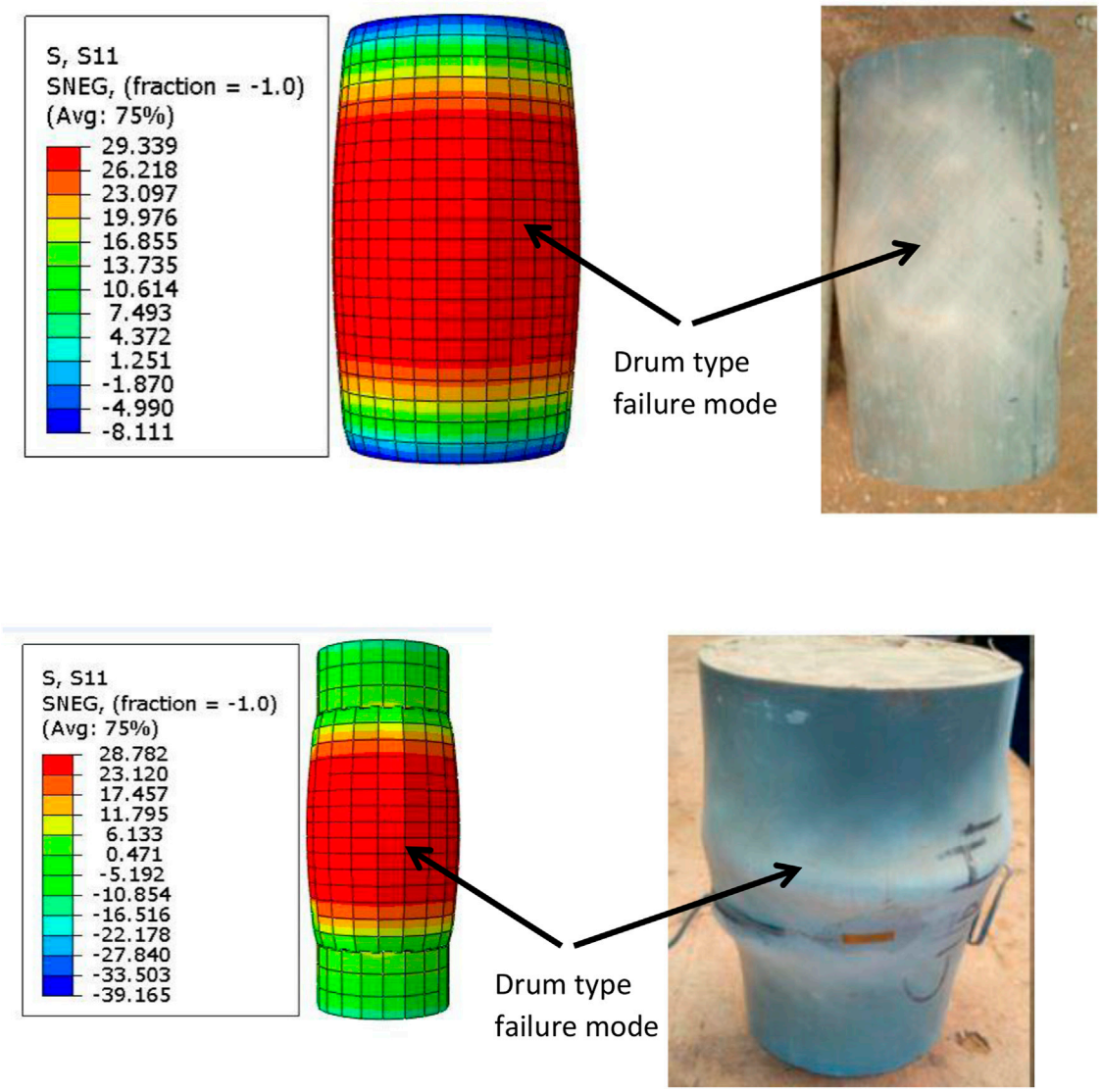

FIGURE 4
Comparison of failure mode of FE and Experimental results. Note: Experimental failure modes were reported by Woldemariam et al. (2019).

means the failure axial load also increased but the rate of failure axial load is less.

With increase in CFRP depth from 158 mm to 338 mm, the failure axial load increased from 294.62 kN to 679.43 kN for layer 1, whereas the failure axial load increased from 518.81 kN to 1178.64 kN for layer 2 having confined concrete strength as 15 MPa. Whereas an increase in confined concrete strength to 25 MPa, the failure axial load is increased from 301.04 kN to 495.83 kN for layer 1 and when the number of layers is increased to 2, the failure axial load is increased from 515.09 kN to 802.39 kN. From Figure 12, it is noted that the increase in confined concrete strength results in an increase in the rate of the failure axial load from 1.48 to 1.65 times for layer 1, whereas the rate of the failure axial load increases from 1.45 to 1.56 times for layer 2. It is also noted that with an increase in the number of layers, there is a decrease in the rate of failure axial load. It is also reported in the literature, that the higher failure axial load is noted for 20 mm CFRP depth for circular columns (Vasumathi et al., 2014).

6.3 Effect of PVC tube thickness

When PVC tube thickness is increased from 2.3 mm to 5.4 mm, failure axial load increased from 1260.62 kN to 820.04 kN for layer 1 for full CFRP wrapping to 100 mm CFRP hoop spacing. When the number of layers is increased to layer 2, the failure axial load

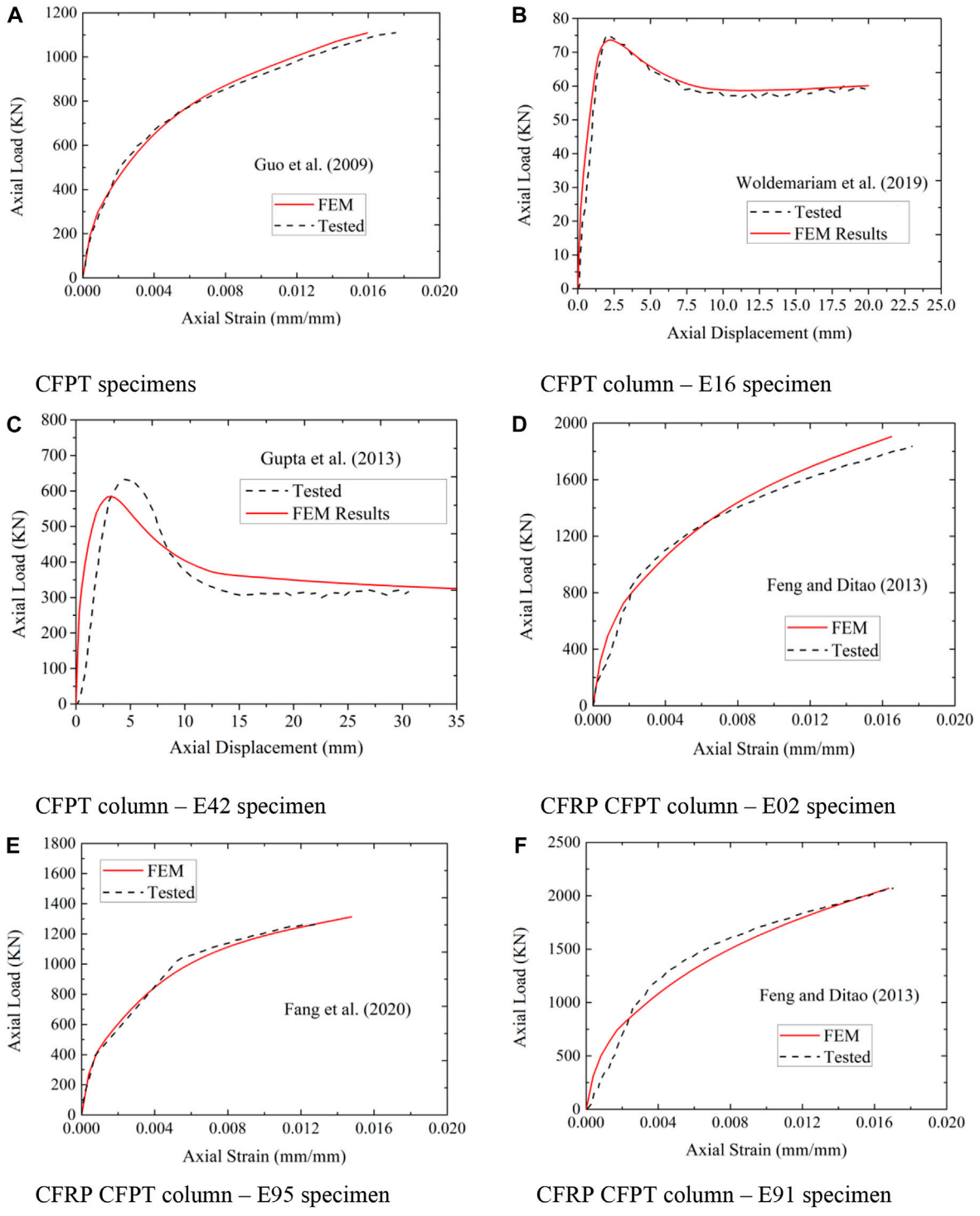

FIGURE 5
Comparison of selected response and FE results of CFPT Specimens.

increases from 1781.51 kN to 866.80 kN for full wrapping to 100 mm CFRP hoop spacing. Failure axial load increased from 2361.59 kN to 889.18 kN for full wrapping to 100 mm CFRP hoop spacing for CFRP layer 3. From Figure 13A, it is noted that for layer 2, the failure axial load increased from 1.41 to 1.06 times when compared to layer 1. Whereas for layer 3, the failure axial load

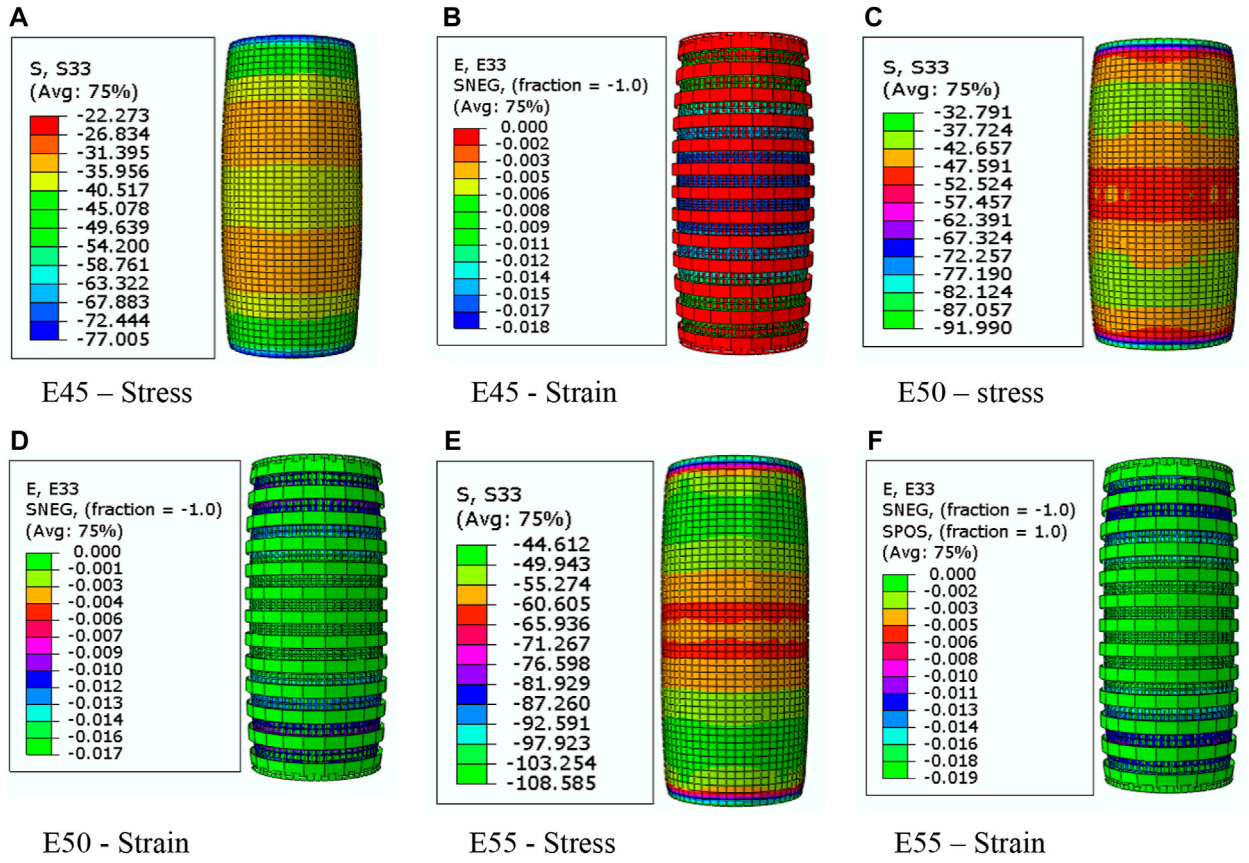

FIGURE 6
Failure modes for CFPT columns without longitudinal reinforcement.

increased from 1.87 to 1.08 times for full CFRP wrapping to 100 mm CFRP hoop spacing for group 8 (part 1, part 2, and part 3).

When PVC tube thickness increased from 2.3 mm to 5.4 mm, the failure axial load increased from 1009.45 kN to 1084.09 kN for 20 mm CFRP hoop spacing having CFRP layer 1. Whereas for 120 mm CFRP hoop spacing, the failure axial load increased from 813.17 kN to 884.89 kN. For layer 2, the failure axial load increased from 1257.69 kN to 1324.90 kN for 20 mm CFRP hoop spacing, and for 120 mm CFRP hoop spacing, the failure axial load increased from 852.02 kN to 928.59 kN. For layer 3, the failure axial load increased from 1492.94 kN to 1572.69 kN for 20 mm CFRP hoop spacing, and for 120 mm CFRP hoop spacing, the failure axial load increased from 873.3 kN to 960.03 kN.

When the number of layers is increased from layer 2 to layer 3, the failure axial load increased by 1.25 times to 1.48 times when compared to layer 1 for 20 mm CFRP hoop spacing. Whereas, for 120 mm CFRP hoop spacing, when the number of layers is increased as 2 and 3, the failure axial load increased 1.22 times and 1.45 times as noted in Figure 13B. An increase in PVC tube thickness results not only increases the failure load-carrying capacity of columns but also influence the stress-strain behavior of the column itself (Abdulla, 2020; Oyawa, et al., 2016). The confinement action of CCFPT columns is reliant on the concrete infill behavior to dilate when loaded, as well as the circular stiffness of the confining member to restrain the enlargement (Oyawa, et al., 2016).

6.4 Effect of column's slenderness ratio

With an increase in the slenderness ratio, there is an increase in axial load is observed in Figure 14A. Failure axial load for slenderness ratio 12.5 with the CFRP hoop spacing as 20, 40, 60, and 100 mm, the load decreases as 999.39, 917.70, 869.74, and 820.04 kN. When the slenderness ratio is increased to 25, the failure axial load increases by 1.010, 1.005, 1.003, and 0.992 times that of the failure axial load for a slenderness ratio of 12.5 for a PVC tube thickness of 2.3 mm. When PVC tube thickness is increased to 3.7 mm, the failure axial load increases by 1.012, 1.006, 1.002, and 0.993 times for a slenderness ratio of 25 when compared to that of the column having a slenderness ratio of 12.5. On further increasing PVC tube thickness to 5.4 mm, the failure axial load increases by 1.015, 1.007, 1.002, and 0.990 times

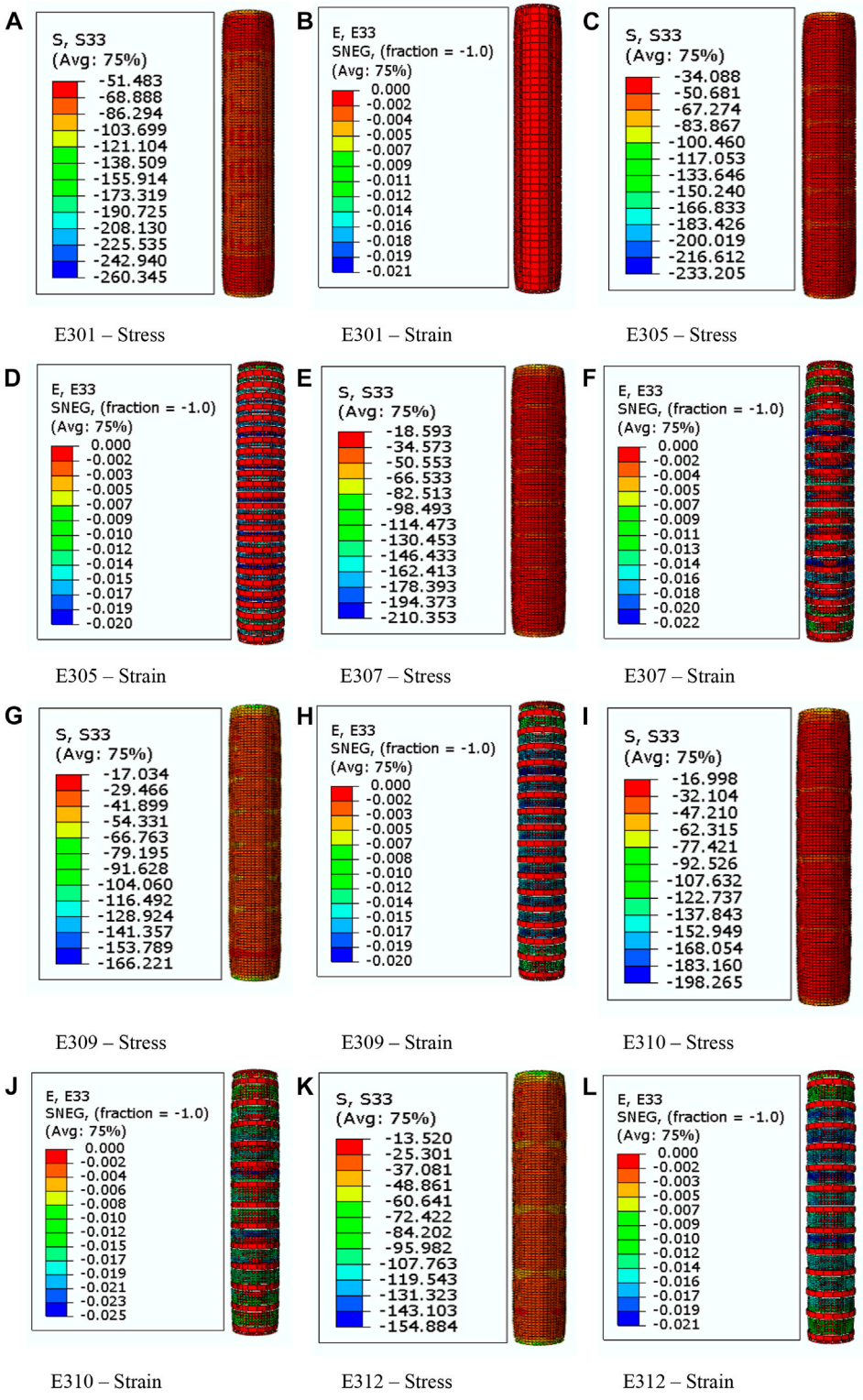

FIGURE 7
Failure modes for CFRP-wrapped CFPT columns with longitudinal reinforcement (Group 12).

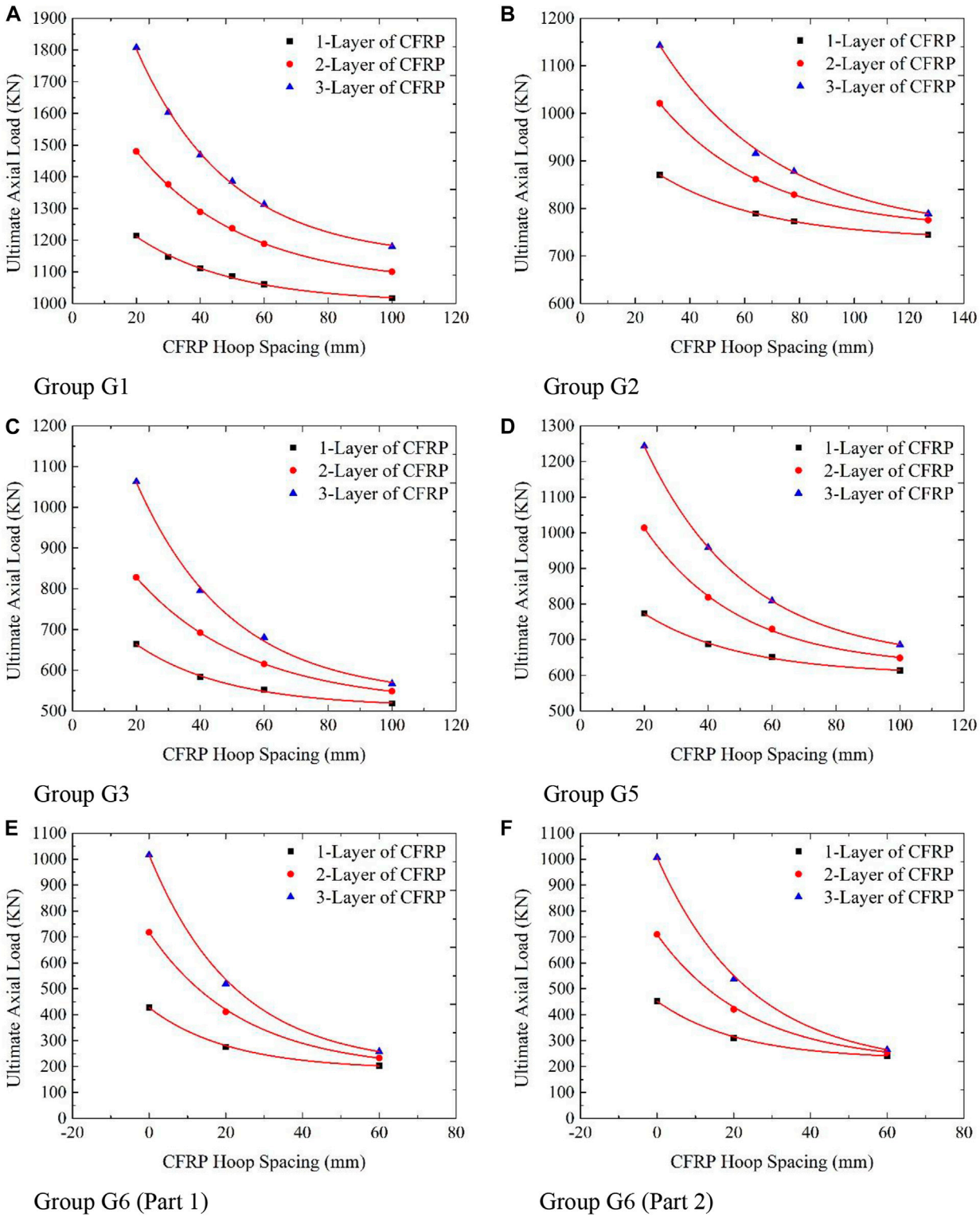

FIGURE 8
Effect of CFRP hoop spacing on failure axial load.

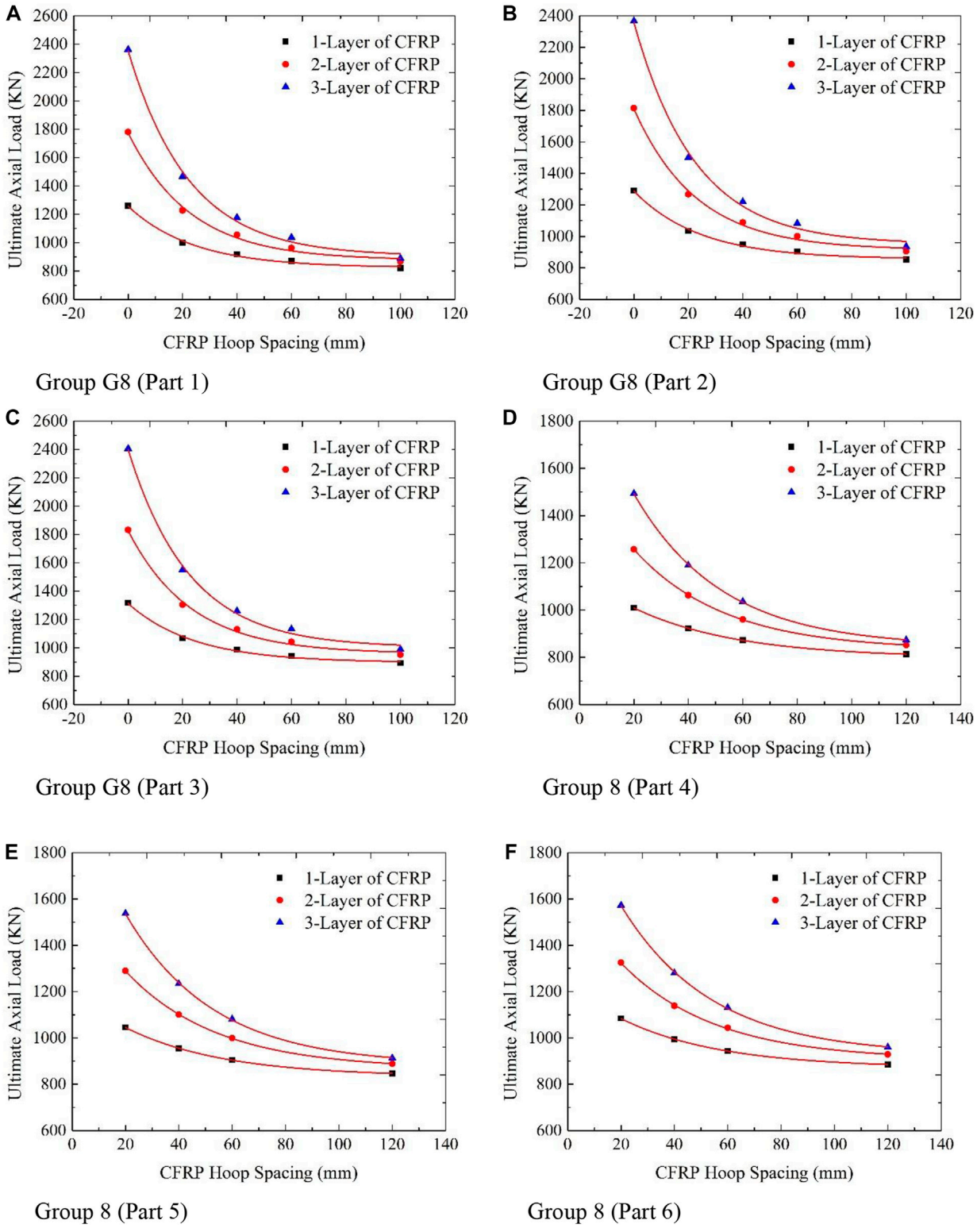

FIGURE 9
Effect of CFRP hoop spacing on failure axial load with steel reinforcement.

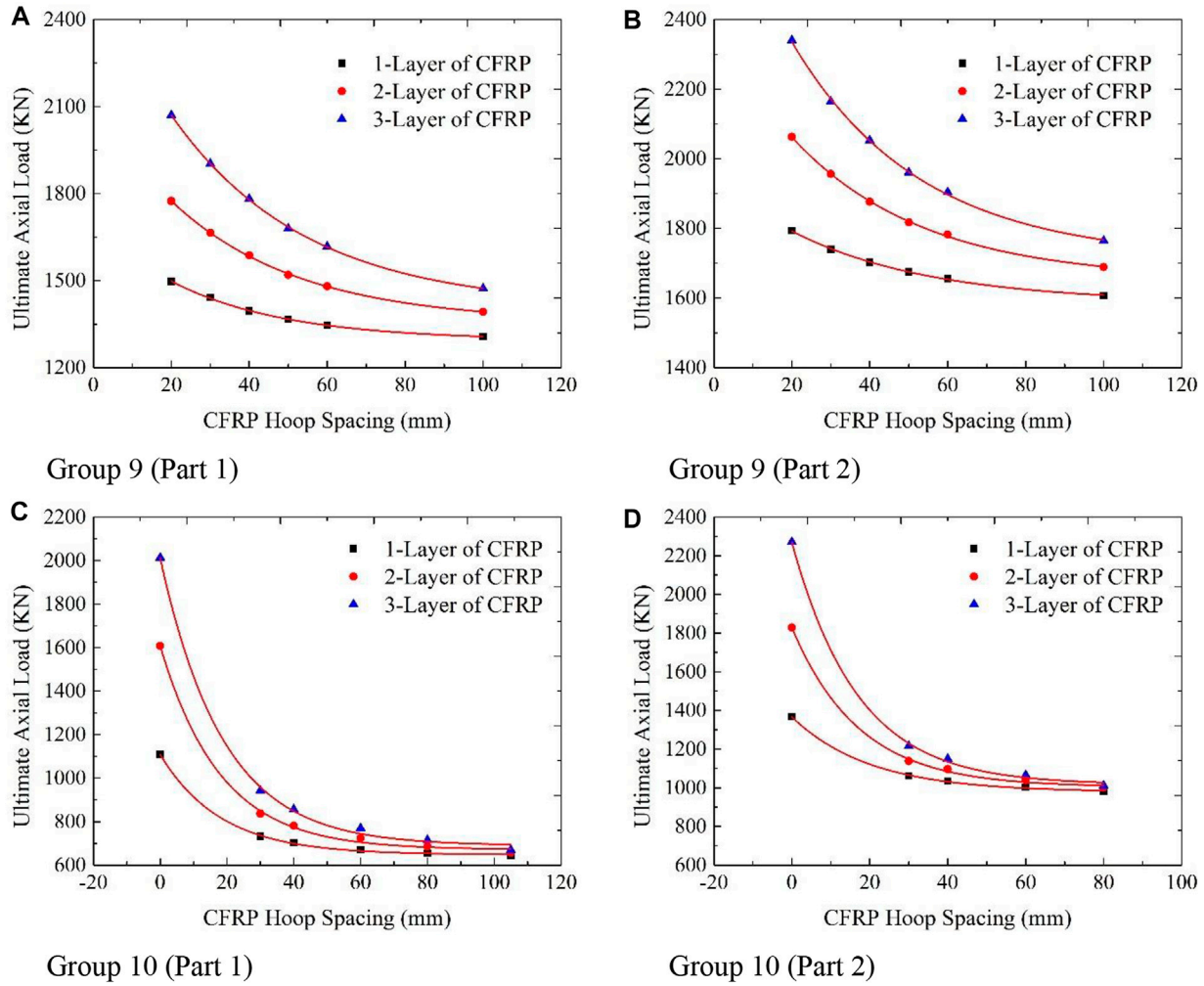

FIGURE 10
Effect of CFRP hoop spacing on axial load.

for a slenderness ratio of 25 when compared to that of columns having a slenderness ratio of 12.5. From this, it can be concluded that, for single-layer CFRP, there is a mild increase in failure axial load when the slenderness ratio is increased twice.

For layer 2, failure axial load for slenderness ratio 12.5 with the CFRP hoop spacing as 20, 40, 60, and 100 mm, the load decreases as 1781.51, 1227.56, 1055.10, and 962.25 kN. When the slenderness ratio is increased to 25, the failure axial load is decreased to 0.706, 0.866, 0.911, and 0.885 times the failure axial load for a slenderness ratio of 12.5 for a PVC tube thickness of 2.3 mm. When PVC tube thickness is increased to 3.7 mm, the failure axial load is decreased to 0.710, 0.868, 0.918, and 0.888 times for a slenderness ratio of 25 when compared to that of a column having a slenderness ratio of 12.5. On further increasing PVC tube thickness to 5.4 mm, the failure axial load is increased as 1.016, 1.006, 1.001, and 0.75 times for a slenderness ratio of 25 when compared to that of columns having a slenderness ratio of 12.5. When the number of CFRP layers is 2, with CFRP depth of 20 mm and 40 mm and PVC tube thickness of 3.7 mm, there is a difference in failure axial load is noted.

From Figure 14B, when CFRP depth is 20 and 40 mm, there is a difference in failure axial load for slenderness ratio is noted. It can be concluded that, with an increase in CFRP depth from 20 mm to 100 mm, there is a decrease in failure axial load is noted with an increase in slenderness ratio. The rate of reduction of failure axial load varies for varying PVC tube thicknesses used.

For three layers of CFRP, the failure axial load behavior is different when compared to two and single-layer CFRP as noted in Figure 14C. Decrease in failure axial load for columns about 6.27% and 3.51% for slenderness ratio of 18.75 and 25 for PVC tube thickness 2.3 mm when compared to columns slenderness

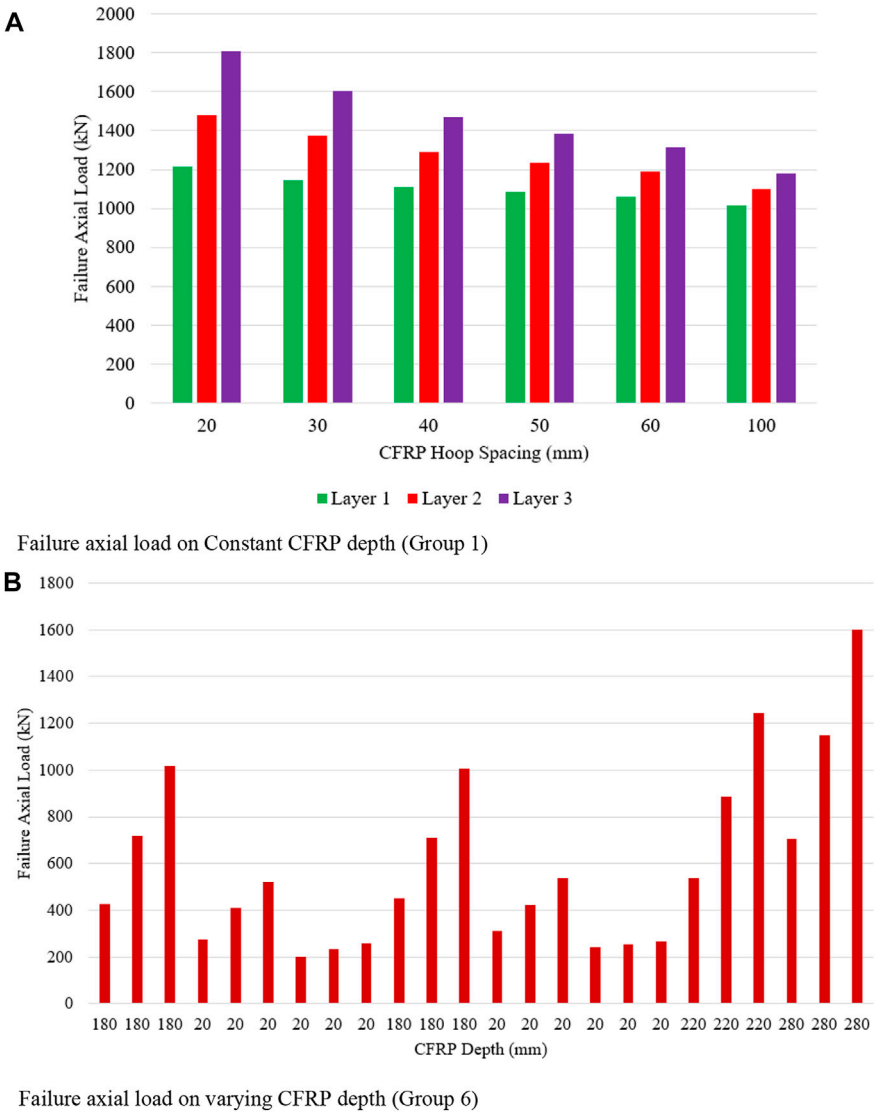

FIGURE 11
Effect of failure axial load on CFRP depth.

ratio of 12.5. Whereas a decrease in failure axial load for 3.7 mm and 5.4 mm is 4.52%, 3.28% and 4.34% and 3.61% for columns having a slenderness ratio of 25 when compared to columns slenderness ratio of 12.5. With an increase in slenderness ratio and increase in PVC thickness, there is a decrease in failure axial load is observed. Whereas from Figure 15, it is noted that with an increase in slenderness ratio, there is an increase in failure axial load and also the rate of increase in failure axial load is slow with an increase in PVC tube thickness observed. With an increase in the slenderness ratio, there is a decrease in the failure axial load capacity of CFPT as reported by Huang, et al. (2022). On a higher slenderness ratio, failure axial load reduction is due to the full utilization of the PVC and concrete material (Huang et al., 2022).

6.5 Effect of CFRP layer

The increase in failure axial load of a column of about 76.09%, 72.69%, and 73.48% for 158, 225, and 338 mm CFRP depth for layer 2, when compared to layer 1 CFRP wrapping, is observed from Figure 16A.

An increase in failure axial load of column specimens of about 71.10% and 61.83% for column specimen diameter as 70 mm and 100 mm for CFRP layer 2 when compared to CFRP layer 1 is observed in Figure 16B. An increase in specimen size with an increase in the number of layers also increases failure axial load. When the number of layers is increased, the failure axial load and failure axial strain of the column specimen is increased as reported by

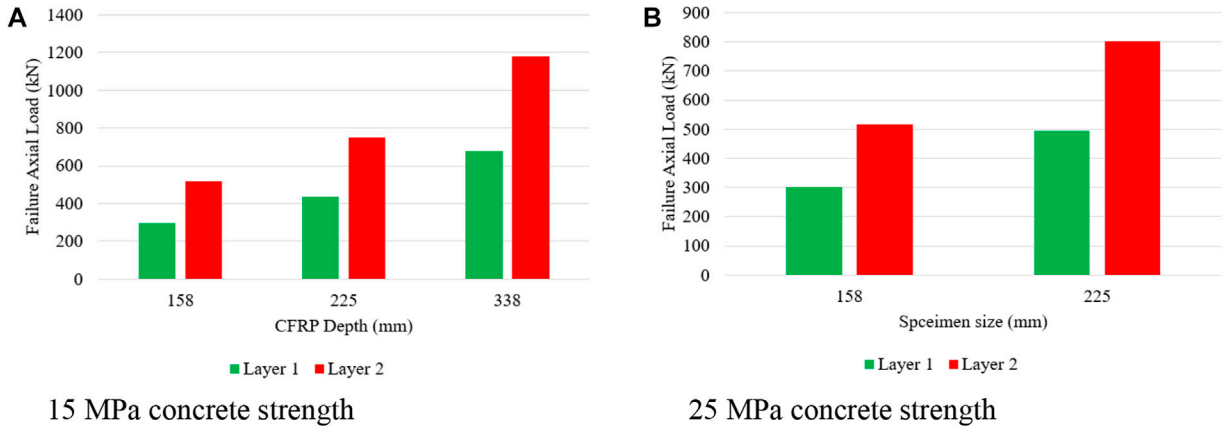

FIGURE 12
Effect of CFRP depth (varying) on axial load (Group 7).

Fakharifar and Chen. (2016). Confining effect of CCFPT increases with an increase in CFRP layers as observed by Jiang et al. (2014).

6.6 Effect of confined concrete strength

An increase in hoop spacing as 20, 40, 60, and 100 mm, for layer 2 results in an increase in failure axial load of about 24.60%, 18.68%, 11.54%, and 5.80% then layer 1 for 28.6 MPa concrete strength is observed from Figure 17A. Whereas for 30 MPa confined concrete strength, there is an increase in failure axial load of 31.00%, 18.99%, 12.11%, and 5.72% for CFRP layer 2 when compared to CFRP layer 1.

On further increase in 34.1 MPa confined concrete strength, there is an increase in failure axial load of 17.25%, 9.11%, 7.30%, and 4.14% for CFRP layer 1 when compared to CFRP layer 2. Increase in confined concrete strength to 43.1 MPa, there is an increase in failure axial load of 22.45%, 12.65%, 9.71%, and 4.04% for CFRP layer 1 when compared to CFRP layer 2. For hoop spacing as 20, 40, 60, and 100 mm, layer 3 results in an increase in failure axial load of about 59.99%, 36.39%, 23.26%, and 9.46% then layer 1 for 28.6 MPa confined concrete strength. On the increase of confined concrete strength to 30 MPa for CFRP layer 3, there is an increase in failure axial load as 60.66%, 39.35%, 24.32%, and 11.83% then CFRP layer 1. On further increase in confined concrete strength to 34.1 MPa for layer 3, there is an increase in failure axial load as 31.21%, 16.00%, 13.59%, and 5.95% then CFRP layer 1. When confined concrete strength is increased to 43.5 MPa for layer 3, there is an increase in failure axial load as 44.86%, 25.63%, 17.80%, and 6.13% then CFRP layer 1 is observed.

It can be observed that the rate of increase in failure axial load is decreased with an increase in confined concrete strength observed for all CFRP layers from Figure 17B. The increase in failure axial load was 45.05%, 14.30%, 11.30%, 7.74%, 4.78%, and 2.01% for CFRP layer 1 for hoop spacing as 0, 30, 40, 60, 80, and 105 mm for 33.6 confined concrete strength then CFRP layer 2 is noted. On the further increase of confined concrete strength to 67.2 MPa for layer 3, there is an increase in failure axial load to 81.54%, 28.75%, 21.93%, 14.62%, and 9.21% then CFRP layer 1. With an increase in the number of layers from layer 1 to layer 3, there is an increase in axial load as twice observed in Figure 17B. When there is an increase in confined concrete strength twice, there is a decrease in failure axial load as twice is noted.

For 28.5 MPa confined concrete strength, for hoop spacing of CFRP layer 2 as 20, 30, 40, 50, 60, and 120 mm, failure axial load increased as 18.50%, 15.53% 13.79%, 11.19%, and 6.55% then layer 1 is observed from Figure 17C. For hoop spacing of CFRP layer 3 as 20, 30, 40, 50, 60, and 120 mm, failure axial load increases by 38.26%, 32.09%, 27.79%, 22.90%, 20.16% and 12.69% then layer 3 is observed for 28.5 confined concrete strength. When there is an increase in confined concrete strength to 45 MPa, the rate of increase in failure axial load is decreased when compared to 28.5 MPa confined concrete strength. From this, it is concluded as an increase in confined concrete strength results in an increase in failure axial load but the rate of increase of load is decreased.

7 Analytical modelling

The analytical expression for the confined concrete relates to the concrete strength, PVC material, hoop reinforcement, and CFRP properties. In particular, the models are proposed to calculate the failure stress which corresponds to important parameters.

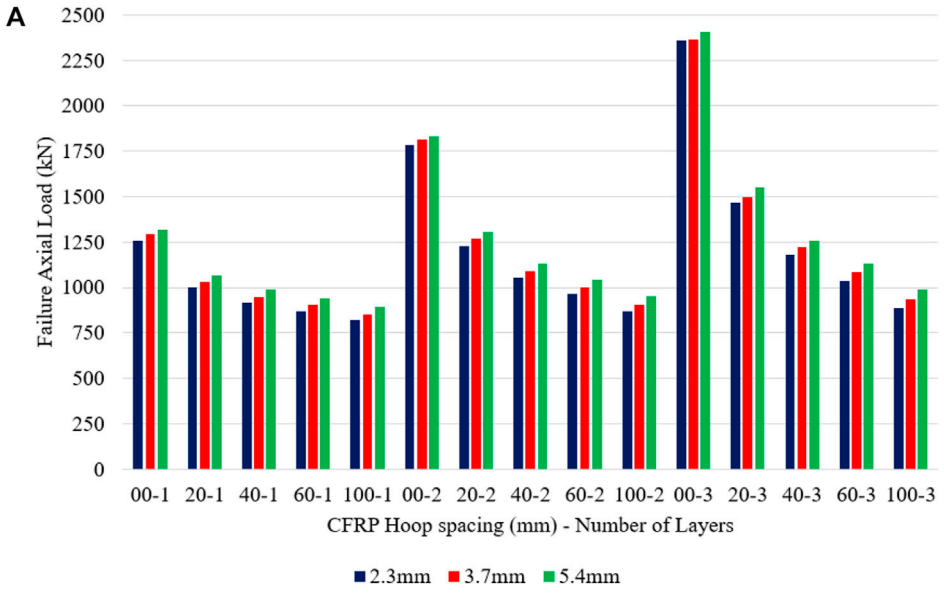

Failure axial load for 31.3 MPa concrete strength Group 8 [part 1, part 2, part 3]

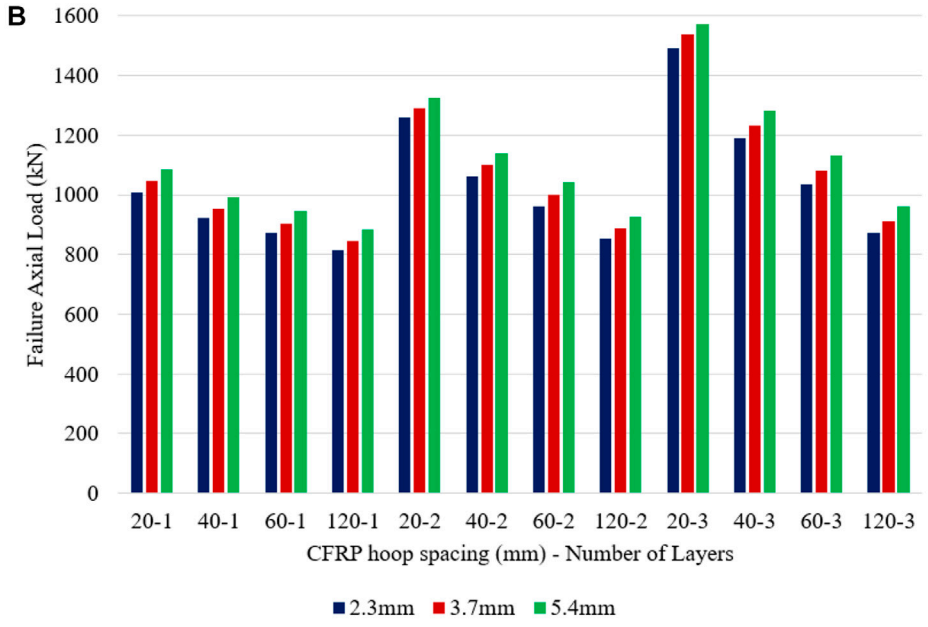

Failure axial load for 36.4 MPa concrete strength Group 8 [part 4, part 5, part 6]

FIGURE 13
Effect of PVC tube thickness.

7.1 Effective lateral confinement pressure

Experimental and FEM tests on CFPT columns have shown that failure stress fcc, is influenced by the longitudinal reinforcing bars, hoop reinforcement bars, and PVC used. Hence, it is necessary to develop a model for determining the failure stress using all these parameters utilizing dimensionless parameters as reported by Wang et al. (2012a). Failure strain of CFRP, the effective rupture strain (ε_{fe}) is the most significant. Hence, rupture strain is

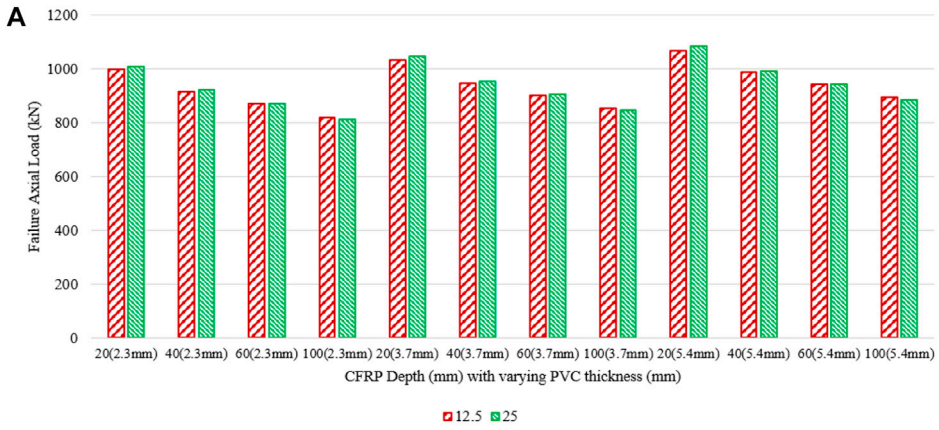

Failure axial load for different PVC thickness and CFRP depth with single layer CFRP

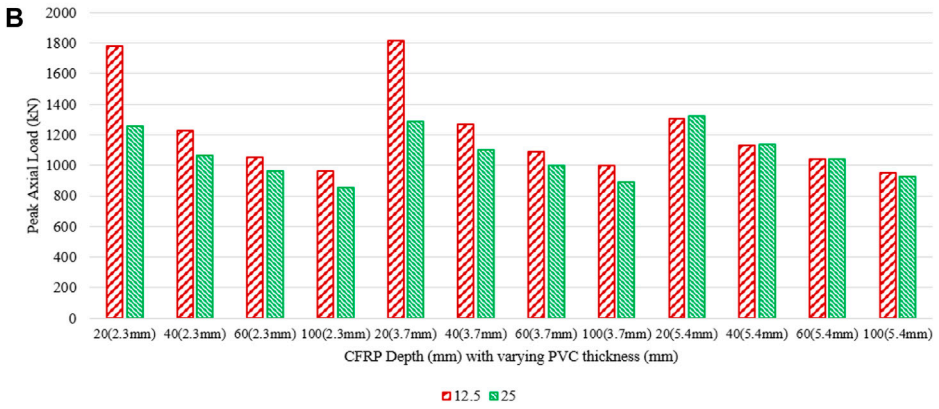

Failure axial load for different PVC thickness and CFRP depth with two layers CFRP

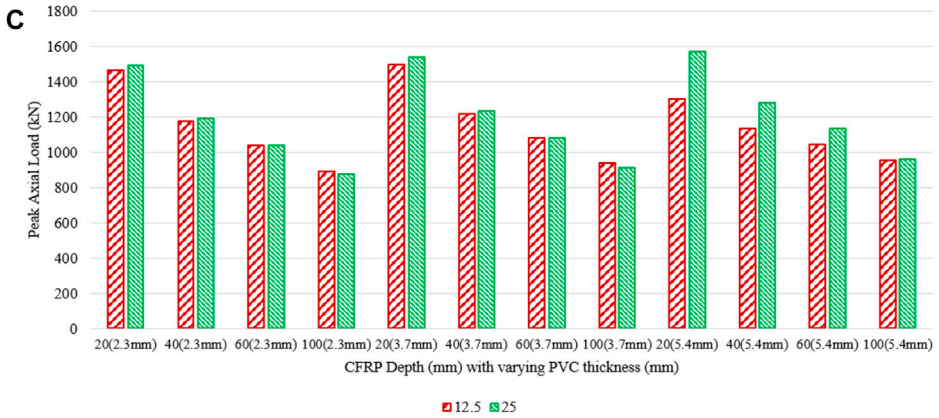

Failure axial load for different PVC thickness and CFRP depth with three layers CFRP

FIGURE 14
Effect of the column's slenderness ratio.

calculated; $\varepsilon_{fe} = K_{\varepsilon}\varepsilon_{fu}$, in which ε_{fu}, is the ultimate tensile strain of CFRP using coupon tests. The confinement effectiveness of the wraps of CFRP was found to increase with extra layers of wrap of CFRP while it decreased with an increase of cross-sectional size. Based on the experimental results found by Wang et al. (2012a), Kε is taken as 0.80.

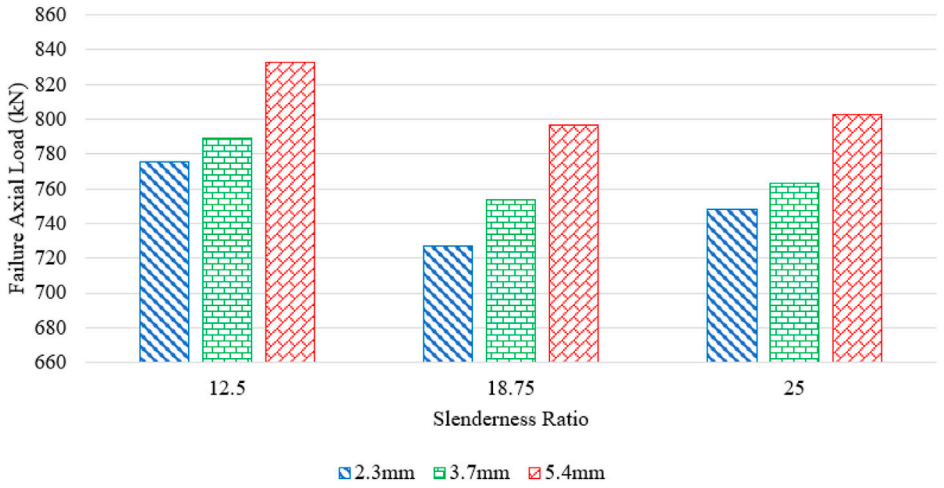

FIGURE 15
Effect of slenderness ratio on failure axial load for different PVC thicknesses.

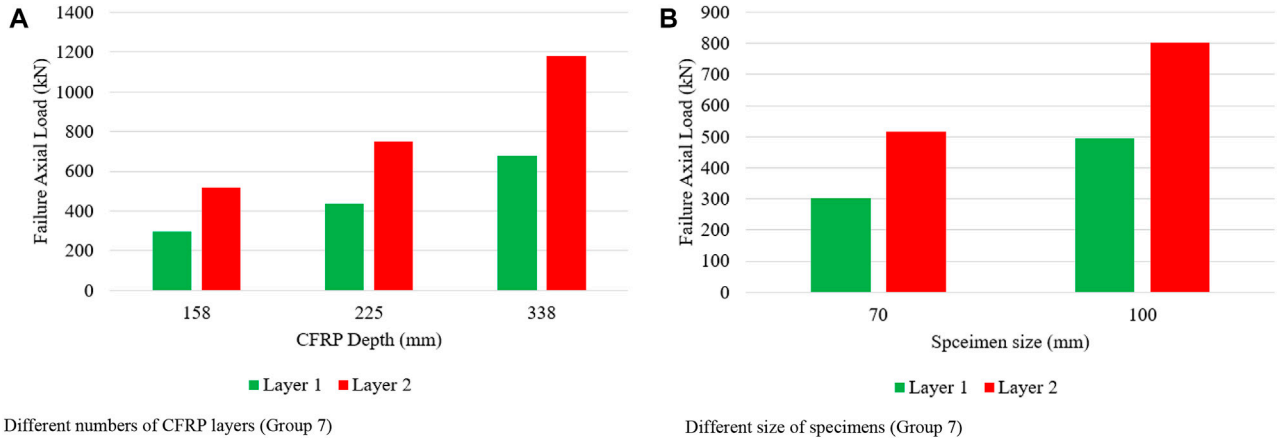

FIGURE 16
Effect of axial load on the different number of CFRP layers.

Similar to Isleem et al. (2018a), there are four different dimensionless parameters are used to develop a model. One more dimensionless parameter was introduced for CFRP as per Hany et al. (2016). Relative to the unconfined compressive strength of concrete, the dimensionless parameters for the PVC (λ_{pvc}), hoop reinforcement (λ_h), longitudinal reinforcement (λ_l), CFRP reinforcement (λ_{CFRP}) are introduced as follows

$$\lambda_{pvc} = \frac{\rho_{pvc} f_{pvc}}{f_{co}} \tag{4}$$

$$\lambda_l = \frac{\rho_{ls} f_{yl}}{f_{co}} \tag{5}$$

$$\lambda_h = \frac{\rho_{hs} f_{yh}}{f_{co}} \tag{6}$$

$$\lambda_{CFRP} = \left(\frac{\rho_{CFRP} E_{CFRP}}{2}\right) \varepsilon_{CFRP,R} \tag{7}$$

Where, ρ_{pvc}, ρ_l, ρ_h and ρ_{CFRP} is the volumetric ratio of PVC tube, longitudinal, hoop reinforcement, and CFRP reinforcement respectively; the volumetric ratio of the PVC tube is calculated as $\rho_{pvc} = \frac{4t}{D}$, t is the thickness of PVC tubes (mm) and D is the diameter of column specimen (mm); the volumetric ratio of the longitudinal

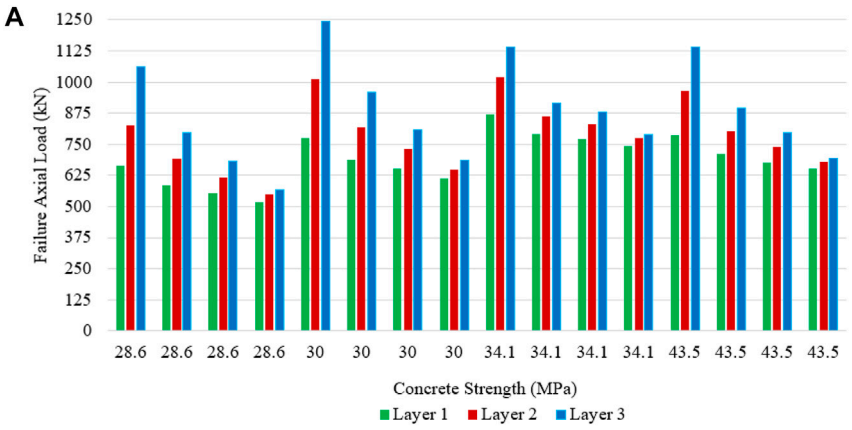

Failure axial load for Group 3, Group 5, Group 2, and Group 4 without longitudinal reinforcement.

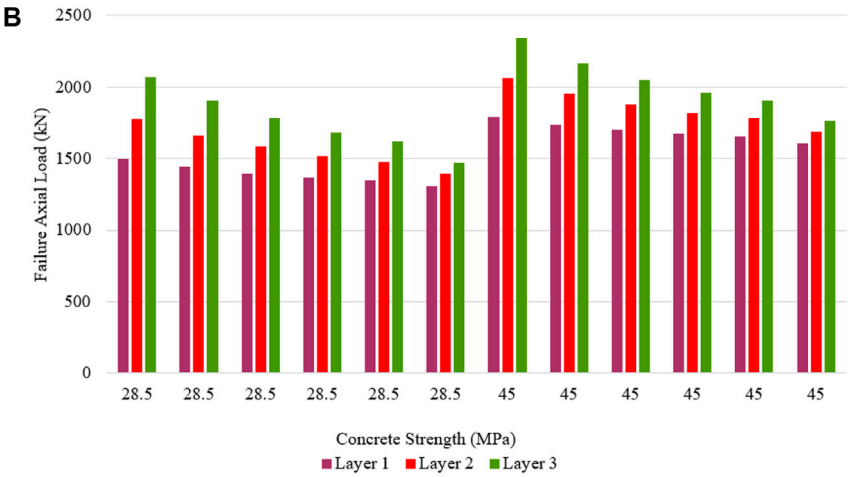

Failure axial load for Group 10 (Part 1) & Group 10 (Part 2) without longitudinal reinforcement

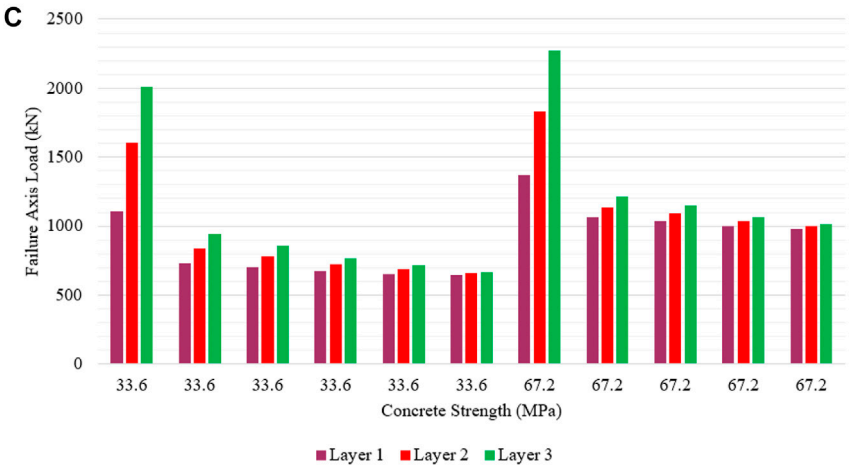

Failure axial load (kN) for Group 9 (Part 1) and Group 9 (Part 2) with longitudinal reinforcement

FIGURE 17
Effect of concrete strength.

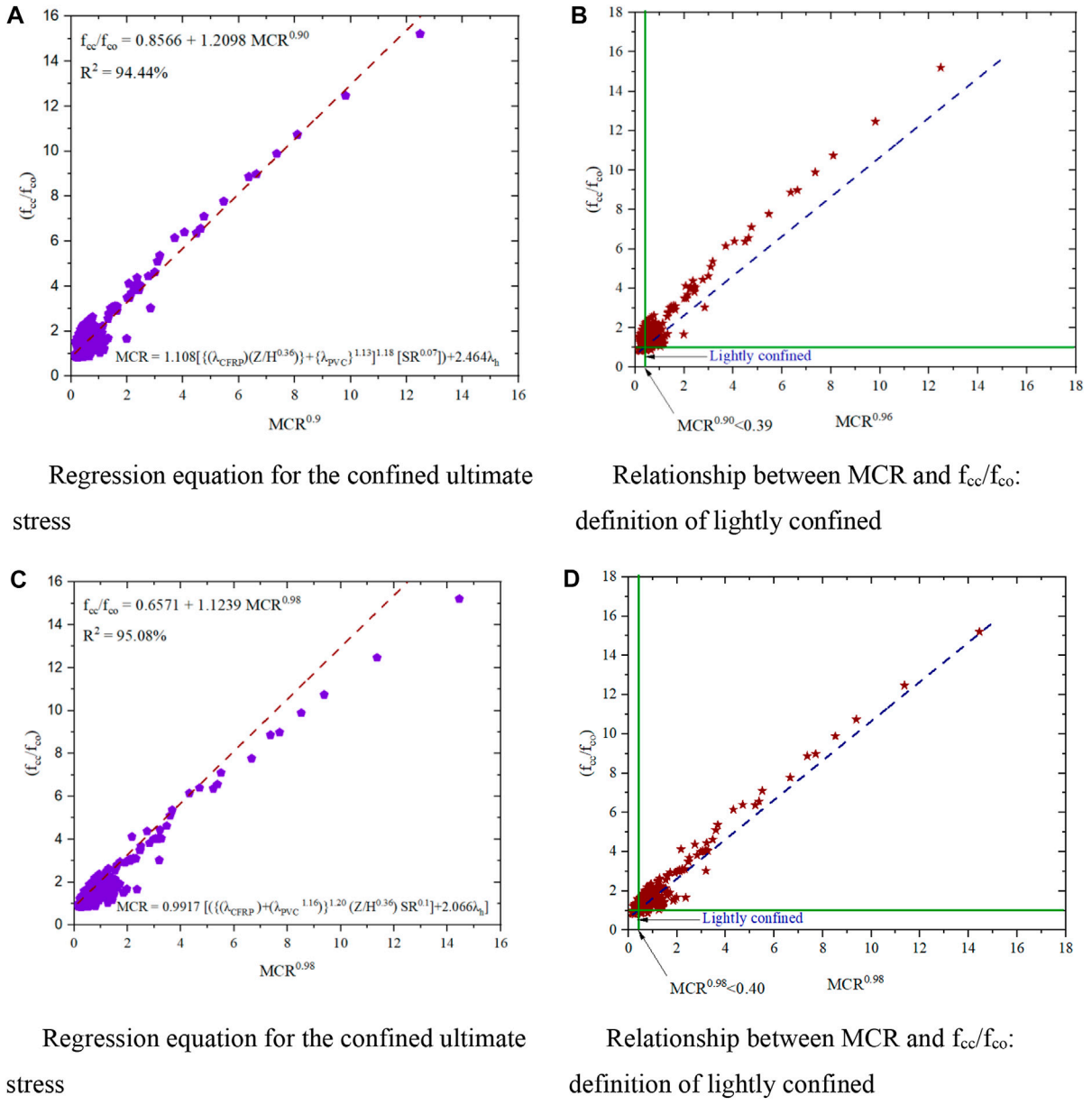

Regression equation for the confined ultimate stress

Relationship between MCR and f_{cc}/f_{co}: definition of lightly confined

Regression equation for the confined ultimate stress

Relationship between MCR and f_{cc}/f_{co}: definition of lightly confined

FIGURE 18
Relationship between MCR and f_{cc}/f_{co} from Eq. 5 **(A)** and **(B)** and MCR and f_{cc}/f_{co} from Eq. 6 **(C)** and **(D)**.

reinforcement is calculated as $\rho_l = \frac{Number\ of\ bars\ x\ rebar\ area}{gross\ sectional\ area}$; the volumetric ratio of the hoop reinforcement is calculated as $\rho_h = \frac{4\ x\ hoop\ rebar\ area}{spacing x\ (D_c - 2xcover)}$; f_{yl} and f_{yh} are yield strength of reinforcement in longitudinal and hoop; f_{pvc} is the PVC yield strength; E_{CFRP} is young's modulus of CFRP; $\varepsilon_{CFRP,\ R}$ is measure strain at which CFRP ruptured in tension. For fully CFRP-wrapped columns, the volumetric ratio is calculated as $\rho_{CFRP} = \frac{4t_{wrap}}{D}$, where D is the diameter of the circular column specimen section. For columns with partially wrapped CFRP, the volumetric ratio is calculated as $\rho_{CFRP} = \frac{4W\ t_{wrap}}{S\ D}$, where W is the width of the CFRP strip and S is the spacing between the CFRP strip (Hany et al., 2016).

7.2 Confinement ratio

An analytical model that considers the influence of the various parameters on CFRP confinement provided to circular

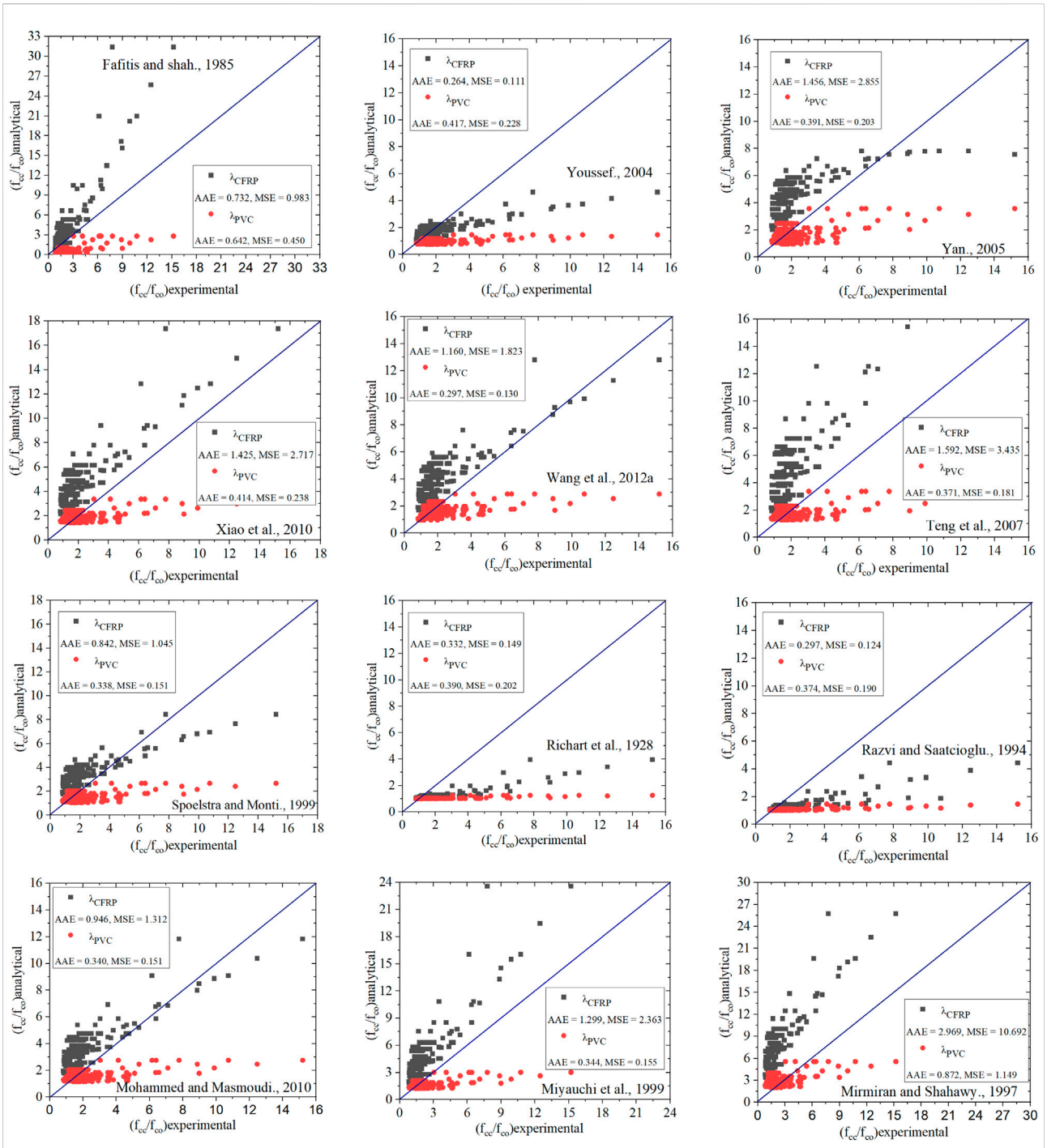

FIGURE 19
(Continued).

PVC columns is now introduced. Ultimate stress f_{cc} and ultimate strain ε_{cc} denote the stress and strain at CFRP rupture failure correspondingly, and they are the two most significant parameters for the stress-strain model of CFRP-confined concrete. The relationship that relates the ultimate stress of CFRP-confined concrete to the various parameters that would

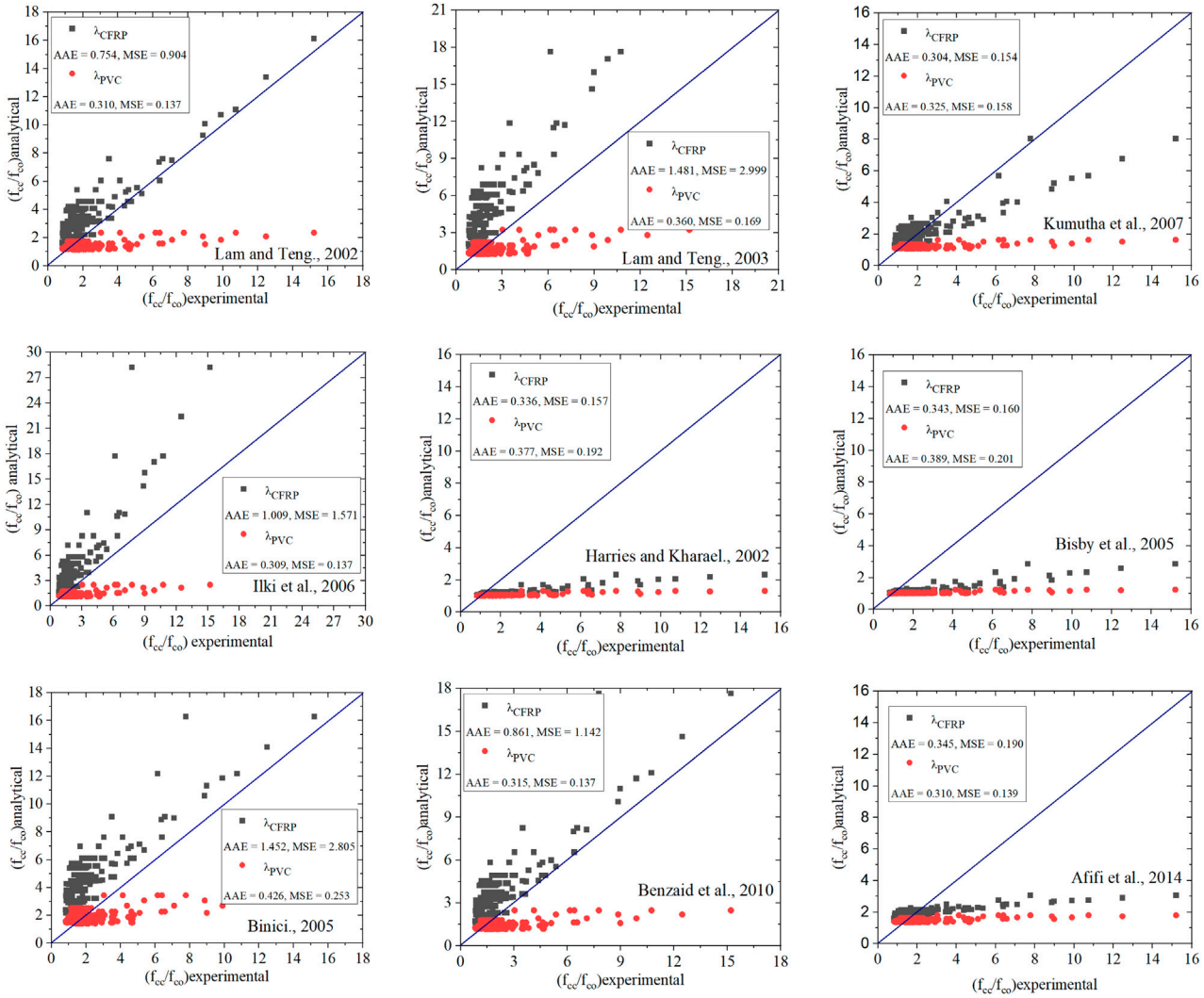

FIGURE 19
(Continued). Evaluation of existing models (based on CFRP-wrapped models) against the test database.

influence its value is mentioned usually as the ultimate strength model. So, in the literature, the relationship between unconfined concrete to confined concrete and longitudinal reinforcement to confined concrete is reported as a linear relationship based on the experimental tests (Wang et al., 2012c).

The following expressions for the failure stress, which depend on the three different dimensionless parameters and slenderness ratio were performed using MINITAB and obtained an R^2 value of 0.95. Z is the clear spacing between the CFRP wrapping used for the analytical model.

$$\frac{f_{cc}}{f_{co}} = 0.7293 + 1.0865\left(\left[\left\{(\lambda_{CFRP})\left(\frac{Z}{H}\right)^{0.41}\right\} + \{\lambda_{PVC}\}^{1.15}\right]^{1.18}[SR^{0.08}]\right) + 2.446\lambda_h \quad (8)$$

$$\frac{f_{cc}}{f_{co}} = \left[0.8486 + 0.9030\left[\left(\left\{(\lambda_{CFRP}) + (\lambda_{PVC})^{1.05}\right\}^{1.25}\left(\frac{Z}{H}\right)^{0.4}\right)SR^{0.1}\right] + 2.140\,(\lambda_h)\right] \quad (9)$$

The effect of the ratio of CFRP wrapping spacing and height of the specimen on the dimensionless parameter λ_{CFRP} separately; λ_{CFRP} and λ_{PVC} respectively are shown in Eqs 8, 9.

7.3 Estimation of CFRP for sufficiently confined concrete

It is known that the effectiveness of CFRP confinement is considerably influenced by three dimensionless parameters which are already discussed in the previous

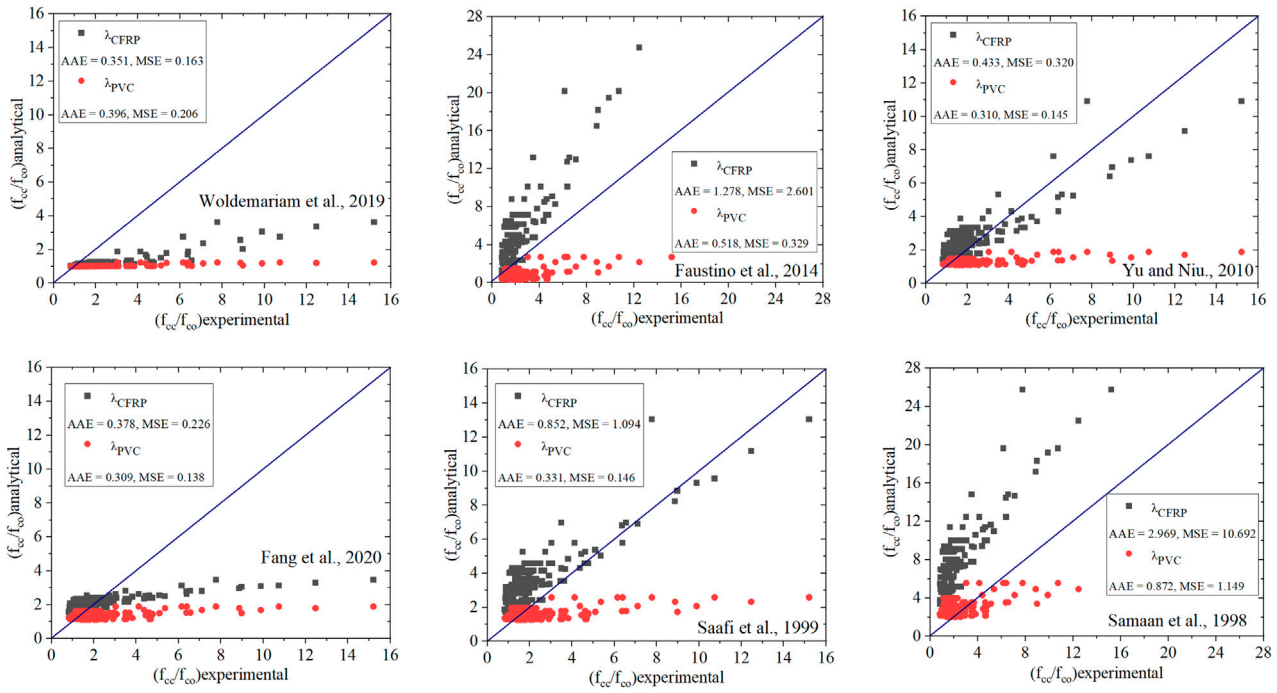

FIGURE 20
Evaluation of existing models (based on PVC CFRP wrapped models) against the test database.

paragraph. Based on multi-parameter regression analysis performed on the test database of 265 specimens, as shown in Figures 18A,B the following expressions (Eqs 10, 11) for assessing the effective CFRP confinement for circular CCFPT columns are therefore proposed, in which the correlation coefficient R^2 is 94.44%. This relationship helps to define the lightly confined as a modified confined ratio (MCR) less than 0.39. Therefore, this limit should not be exceeded in practice because it is an ineffective use of CFRP wrap around concrete-filled PVC tube columns.

$$\frac{f_{cc}}{f_{co}} = 0.8566 + 1.2098\,(MCR)^{0.90} \tag{10}$$

$$MCR = 1.108\left(\left[\left\{(\lambda_{CFRP})\left(\frac{Z}{H}\right)^{0.36}\right\} + \{\lambda_{PVC}\}^{1.13}\right]^{1.18}[SR^{0.07}]\right) + 2.464\lambda_h \tag{11}$$

Another multi-parameter regression analysis was performed on the test database and relationships have arrived as shown in Figures 18C,D those relationships are stated in Eqs 12, 13.

$$\frac{f_{cc}}{f_{co}} = 0.6571 + 1.1239\,(MCR)^{0.98} \tag{12}$$

$$MCR = \left[0.9917\left[\left(\{(\lambda_{CFRP}) + (\lambda_{PVC})^{1.16}\}^{1.20}\left(\frac{Z}{H}\right)^{0.36}\right)SR^{0.1}\right] + 2.066\,(\lambda_h)\right] \tag{13}$$

For assessing the effective CFRP confinement CCFPT columns are therefore proposed, in which the corresponding coefficient of relation is obtained as 95.08%.

8 Evaluation of exiting strength models

The precision of the proposed confinement model for PVC-CFRP columns and other pertinent models accessible in the previous literature was evaluated (Isleem et al., 2022) using two statistical indicators–the average absolute error (AAE) and the mean square error (MSE), are given by

$$AAE = \frac{\sum_{i=1}^{n}\left|\frac{mod_i - exp_i}{exp_i}\right|}{n_s} \tag{14}$$

$$\mathrm{MSE} = \frac{\sum_{i=1}^{n}\left[\frac{mod_i - exp_i}{exp_i}\right]^2}{n_s} \tag{15}$$

Where, $\mathrm{Mod_i}$ is the model value and $\mathrm{exp_i}$ is the analytical value obtained from the model and experimental measured from specimen i and n_s is the total number of test specimens. To compare the different models available for CFRP-

wrapped columns and assess their precision in predicting the ultimate strengths. Figure 19 shows a comparison between the analytical and experimental results for the required specimens listed in Table 2. Another comparison of the models available in PVC CFRP-wrapped columns and evaluate their accuracy in predicting the ultimate strengths are shown in Figure 20. Different models from the literature available for CFRP wrapped and CFPT columns show poor relation when compared to the model proposed in Eqs 10, 12.

9 Conclusion

In this study, simulated work on CFPT columns was done to check the appropriateness and concert of CFPT columns for structural applications is analyzed. We took 44 specimens from the literature to determine the ultimate load and ultimate strain from FEM software. CFPT columns are wrapped with CFRP fully or partially for both reinforced or unreinforced specimens and simulated using FEM software to determine the ultimate axial load and ultimate axial strain. Analytical models are developed for predicting ultimate axial load and ultimate axial strain and validated using models available in the literature. Based on the research, the following conclusions are made:

- An increase in hoop spacing results in decreases in ultimate axial load. The rate of ultimate axial load decreases with an increase in the number of layers.
- For constant depth of CFRP layer, the ultimate axial load decreases with increased hoop spacing
- For varying depths of the CFRP layer, the ultimate axial load increases with an increase in CFRP layer depth
- An increase in the number of layers increases the ultimate axial load increasing with an increase in PVC tube thickness
- An increase in hoop spacing of the CFRP wrap layer results in the ultimate axial load decrease with an increase in PVC tube thickness
- No clear conclusion can be drawn for the slenderness ratio of the column, for the ultimate axial load
- An increase in the number of CFRP layers results increase in ultimate axial load, with an increase in CFRP depth and column specimen size
- An increase in confined concrete strength increases the ultimate axial load.
- The ultimate stress model is developed for CFRP CFPT columns with help of dimensionless parameters
- The threshold limit for the Modified Confined Pressure ratio for CFRP CFPT columns is developed

This kind of new composite structure has a specific area of application in the construction field subjected to severe exposure conditions of columns and subjected to high lateral loading. CFRP CFPT columns provide a better solution for the columns subjected to lateral loading and poor durability conditions.

Data availability statement

The raw data supporting the conclusion of this article will be made available by the authors, without undue reservation.

Author contributions

Conceptualization: HI, investigation: HI and PJ, methodology: HI and PJ, project administration: HI and PJ, resources: HI and PJ, software: HI and PJ, supervision: HI, validation: PJ, visualization: PJ, SQ, FA, CR, and HN, writing–original draft: PJ, SQ, FA, writing–review and editing: PJ, SQ, FA, and CR, Funding: MS.

Acknowledgments

The authors greatly appreciate the support from Qujing Normal University, Qujing, Yunnan, China, for facilitating the structural concrete laboratory. The authors acknowledge that the research is partially funded by the Ministry of Science and Higher Education of the Russian Federation as part of the World Class Research Center Program: Advanced Digital Technologies (Contract No. 075-15-2022-311 dated 20.04.2022).

Conflict of interest

The authors declare that the research was conducted in the absence of any commercial or financial relationships that could be construed as a potential conflict of interest.

Publisher's note

References

ABAQUS (2014). ABAQUS version 6.14-2. Providence, RI, USA: Dassault systèmes, simulia, 440. Available at: https://www.3ds.com.

Abbasnia, R., Ahmadi, R., and Ziaadiny, H. (2012). Effect of confinement level, aspect ratio and concrete strength on the cyclic stress-strain behavior of FRP-confined concrete prisms. *Compos. Part B Eng.* 43 (2), 825–831. doi:10.1016/j.compositesb.2011.11.008

Abbassi, F., and Ahmad, F. (2020). Behavior analysis of concrete with recycled tire rubber as aggregate using 3D-digital image correlation. *J. Clean. Prod.* 274, 123074. doi:10.1016/j.jclepro.2020.123074

Abdulla, N. A. (2020). The behaviour of concrete-filled plastic tube under axial compression. *Jordon J. Civ. Eng.* 14 (1), 69–81.

ACI Standards (2019). *Building conde requirements for structural concrete*. United States: American Concrete Institute.

Aksoylu, C., Özkılıç, Y, O., Madenci, E., and Safonov, A. (2022). Compressive behavior of pultruded GFRP boxes with concentric openings strengthened by different composite wrappings. *Polymers* 14, 4095. doi:10.3390/polym14194095

Alatshan, F., Altomate, A., and Hamad, S. (2022). Concrete filled plastic stub columns strength under axial compression. *Open J. Civ. Eng.* 12, 87–100. doi:10.4236/ojce.2022.121007

Bandyopadhyay, A., Samanta, A. K., Michel, A. K., and Paul, K. J. (2019). Assessment of axial capacity of RC stub column confined with unplasticized polyvinyl chloride pipe. *J. Inst. Eng. India. Ser. A* 100 (4), 535–546. doi:10.1007/s40030-019-00397-5

Chang, Y., Chen, W., Xiao, Q., Rong, E., and Peng, L. (2021). Theoretical and experimental study on axial compression concrete-filled tubes with different confinements. *J. Constr. Steel Res.* 185, 106862. doi:10.1016/j.jcsr.2021.106862

Fakharifar, M., and Chen, G. (2016). Compressive behavior of FRP-confined concrete-filled PVC tubular columns. *Compos. Struct.* 141, 91–109. doi:10.1016/j.compstruct.2016.01.004

Fakharifar, M., and Chen, G. (2017). FRP confined concrete filled PVC tubes: A new design concept for ductile columns construction in seismic regions. *Constr. Build. Mater.* 130, 287–302. doi:10.1016/j.conbuildmat.2016.11.056

Fang, F., Yu, F., Guan, Y., Wang, Z., Feng, C., and Li, D. (2020). A model for predicting the stress–strain relation of PVC-CFRP confined concrete stub columns under axial compression. *structures* 26, 259–270. doi:10.1016/j.istruc.2020.04.023

Feng, Y., and Ditao, N. (2013). Experimental study on PVC-CFRP confined reinforced concrete short column under axial compression. *J. Build. Struct.* 34 (6), 129–137.

Gao, C., Huang, L., Yan, L., Jin, R., and Kasal, B. (2019). Strength and ductility improvement of recycled aggregate concrete by polyester FRP-PVC tube confinement. *Compos. Part B Eng.* 162, 668–676. doi:10.1016/j.compositesb.2018.10.102

Gemi, L., Alsdudi, M., Aksoylu, C., Yazman, S., Özkılıç, Y, O., and Arslan, M. H. (2022b). Optimum amount of CFRP for strengthening shear deficient reinforced concrete beams. *steel Compos. Struct.* 43 (6), 735–757. doi:10.12989/scs.2022.43.6.735

Gemi, L., Madenci, E., Özkılıç, Y, O., Yazman, S., and Safonov, A. (2022). Effect of fiber wrapping on bending behavior of reinforced concrete filled pultruded GFRP composite hybrid beams. *Polymers* 14, 3740. doi:10.3390/polym14183740

Guo, Y. C., Huang, P. Y., Yang, Y., and Li, L. J. (2008). Experimental studies on axially loaded concrete columns confined by different materials. *Adv. Concr. Struct.* 400, 513. doi:10.4028/www.scientific.net/KEM.400-402.513

Gupta, P. K. (2013). Confinement of concrete columns with unplasticized Poly-Vinyl Chloride tubes. *Int. J. Adv. Struct. Eng.* 5 (19), 19. doi:10.1186/2008-6695-5-19

Gupta, P. K., and Verma, V. K. (2014). Study of concrete filled unplasticized polyvinyl chloride tubes in marine environment. *Proc. institutions Mech. Eng. Part M J. Eng. Marit. Environ.* 230. doi:10.1177/1475090214560448

Hadi, M. N. S. (2009). Behaviour of eccentric loading of FRP confined fibre steel reinforced concrete columns. *Constr. Build. Mat.* 23, 1102–1108. doi:10.1016/j.conbuildmat.2008.05.024

Han, L. H., Li, W., and Bjorhovde, R. (2014). Developments and advanced applications of concrete-filled steel tubular (CFST) structures: Members. *J. Constr. Steel Res.* 100, 211–228. doi:10.1016/j.jcsr.2014.04.016

Hany, N. F., Hantouche, E. G., and Harajli, M. H. (2016). Axial stress-strain model of CFRP confined concrete under monotonic and cyclic loading. *J. Compos. Constr.* 19, 104015004. doi:10.1061/(ASCE)CC.1943-5614.0000557

Harajli, M. H. (2006). Axial stress-strain relationship for FRP confined circular and rectangular concrete columns. *Cem. Concr. Compos.* 28, 938–948. doi:10.1016/j.cemconcomp.2006.07.005

Huang, Y., Li, W., Lu, Y., Liang, H., and Yan, Y. (2022). Behaviour of CFST slender columns strengthened with steel tube and sandwiched concrete jackets under axial loading. *J. Build. Eng.* 45, 103613. doi:10.1016/j.jobe.2021.103613

Isleem, H. F., Wang, D., and Wang, Z. (2018b). Modeling the axial compressive stress-strain behavior of CFRP-confined rectangular RC columns under monotonic and cyclic loading. *Compos. Struct.* 185, 229–240. doi:10.1016/j.compstruct.2017.11.023

Isleem, H. F., Wang, Z., Wang, D., and Smith, S. T. (2018a). Monotonic and cyclic axial compressive behavior of CFRP-confined rectangular RC columns. *J. Compos. Constr.* 22 (4), 04018023. doi:10.1061/(ASCE)CC.1943-5614.0000860

Isleem, H. F., Jagadesh, P., Ahmad, J., Qaidi, S., Althoey, F., and Mohammed Najm, H. (2022). Finite element and analytical modelling of PVC-confined concrete columns under axial compression. *Front. Mat.* 9, 1011675. doi:10.3389/fmats.2022.1011675

Jackubowicz, I., Yaramadi, N., and Gevert, T. (1999). Effects of accelerated and natural ageing on plasticized polyvinyl chloride (PVC). *Polym. Degrad. Stab.* 66 (3), 415–421. doi:10.1016/s0141-3910(99)00094-4

Jiang, S. F., Ma, S. L., and Wu, Z. Q. (2014). Experimental study and theoretical analysis on slender concrete-filled CFRP–PVC tubular columns. *Constr. Build. Mater.* 53, 475–487. doi:10.1016/j.conbuildmat.2013.11.089

Jin, L., Chen, H., Wang, Z., and Du, X. (2020). Size effect on axial compressive failure of CFRP wrapped square concrete columns, tests and simulations. *Compos. Struct.* 254, 112843. doi:10.1016/j.compstruct.2020.112843

Kazmi, S. M. S., Munir, M. J., and Wu, Y. F. (2021). Application of waste tire rubber and recycled aggregates in concrete products: A new compression casting approach. *Resour. Conserv. Recycl.* 167, 105353. doi:10.1016/j.resconrec.2020.105353

Mammen, A. M., and Antony, M. (2017). "Experimental study on the axial compression of GRP concrete PVC tube composite columns," in IOP conference series: Earth and Environmental science, Makassar, Indonesia, October 25–26, 2017, 042013. IOP Publishing.

Masia, M. J., Gale, T. N., and Shrive, N. G. (2004). Size effects in axially loaded square-section concrete prisms strengthened using carbon fibre reinforced polymer wrapping. *Can. J. Civ. Eng.* 31 (1), 1–13. doi:10.1139/l03-064

Mhanna, H. H., Hawileh, R. A., and Abdalla, J. A. (2020). Shear strengthening of reinforced concrete T-beams using CFRP laminates anchored with bent CFRP splay anchors. *Procedia Struct. Integr.* 28, 811–819. doi:10.1016/j.prostr.2020.10.095

Micelli, F., Mazzotta, R., Leone, M., and Aiello, M. A. (2015). Review study on the durability of FRP-Confined concrete. *J. Compos. Constr.* 19 (3), 04014056. doi:10.1061/(asce)cc.1943-5614.0000520

Nowack, R., Otto, O. I., and Braun, E. W. (1995). *Jahre Erfahrungen mit Rohrleitungen aus weichmacherfreiem Poly Vinyl Chrloride (PVC-U)*. Alphacan omiplast: KRV Nachrichte, 1–95.

Oyawa, W. O., Gathimba, N. K., and Manguriu, G. N. (2016). Structural response of composite concrete filled plastic tubes in compression. *Steel compos. Struct.* 21 (3), 589–604. doi:10.12989/scs.2016.21.3.589

Ozbakkaloglu, T., and Vincent, T. (2014). Axial compressive behavior of circular high-strength concrete-filled FRP tubes. *J. Compos. Constr.* 18 (2), 04013037. doi:10.1061/(asce)cc.1943-5614.0000410

Ozkilic, Y. O., Aksoylu, C., and Arslan, M. H. (2021c). Experimental and numerical investigations of steel fiber reinforced concrete dapped end purlins. *J. Build. Eng.* 36, 102119. doi:10.1016/j.jobe.2020.102119

Ozkilic, Y. O., Aksoylu, C., and Arslan, M. H. (2021a). Numerical evaluation of effects of shear span, stirrup spacing and angle of stirrup on reinforced concrete beam behaviour. *Struct. Eng. Mech.* 79 (3), 309–326. doi:10.12989/sem.2021.79.3.309

Ozkilic, Y. O., Aksoylu, C., Yazman, S., Gemi, L., and Arslan, M. H. (2022). Behavior of CFRP-strengthened RC beams with circular web openings in shear zones: Numerical study. *Structures* 41, 1369–1389. doi:10.1016/j.istruc.2022.05.061

Ozkilic, Y. O., Yazman, S., Aksoylu, C., Arslan, M. H., and Gemi, L. (2021b). Numerical investigation of the parameters influencing the behavior of dapped end prefabricated concrete purlins with and without CFRP strengthening. *Constr. Build. Mater.* 275, 122173. doi:10.1016/j.conbuildmat.2020.122173

Papanikolaou, V. K., and Kappos, A. J. (2007). Confinement-sensitive plasticity constitutive model for concrete in triaxial compression. *Int. J. Solids Struct.* 44, 7021–7048. doi:10.1016/j.ijsolstr.2007.03.022

Ping, Y. L., and Peng, F. (2006). Applications and development of fiber-reinforced polymer in engineering structures. *China Civ. Eng. J.* 39, 25–36. doi:10.3390/fib10030027

Raza, A., Khan, Q. U. Z., and Ahmad, A. (2019). Numerical investigation of load-carrying capacity of GFRP reinforced rectangular concrete members using CDP model in ABAQUS. *Adv. Civ. Eng.* 2019, 1745341–1745421. doi:10.1155/2019/1745341

Rocca, S. (2007). "Experimental and analytical evaluation of FRP-confined large-size reinforced concrete columns," (United States: Univ. of Missouri-Rolla). Ph.D. thesis.

Teng, J. G., Huang, Y. L., Lam, L., and Ye, L. P. (2007). Theoretical model for fiber reinforced polymer-confined concrete. *J. Compos. Constr.* 11 (2), 201–210. doi:10.1061/(asce)1090-0268(2007)11:2(201)

Toutanji, H., and Sennah, M. (2002). Stress-strain behavior of concrete columns confined with hybrid composite materials. *Mat. Struct.* 35 (6), 338. doi:10.1617/13653

Vasumathi, A. M., Raj Kumar, K., and Ganesh Prabhu, G. (2014). Compressive behaviour of RC column with fibre reinforced concrete confined by CFRP strips. *Adv. Mater. Sci. Eng.* 2014, 601915. doi:10.1155/2014/601915

Vedernikov, A., Gemi, L., Madenci, E., Özkılıç, Y, O., Yazman, S., Gusev, S., et al. (2022). Effects of high pulling speeds on mechanical properties and morphology of pultruded GFRP composite flat laminates. *Compos. Struct.* 301, 116216. doi:10.1016/j.compstruct.2022.116216

Wang, J., and Yang, Q. (2010). Experimental study on mechanical properties of concrete confined with plastic pipe. *ACI Mater. Journals* 107, 132. doi:10.14359/51663576

Wang, L. M., and Wu, Y. F. (2008). Effect of corner radius on the performance of CFRP-confined square concrete columns: Test. *Eng. Struct.* 30 (2), 493–505. doi:10.1016/j.engstruct.2007.04.016

Wang, Z., Wang, D., Smith, S. T., and Lu, D. (2012c). Experimental testing and analytical modeling of CFRP confined large circular RC columns subjected to cyclic axial compression. *Eng. Struct.* 40, 64–74. doi:10.1016/j.engstruct.2012.01.004

Wang, Z. Y., Wang, D. Y., Smith, S. T., and Lu, D. G. (2012a). CFRP confined square RC columns. I: Experimental investigation. *J. Compos. Constr.* 16 (2), 150–160. doi:10.1061/(ASCE)CC.1943-5614.0000245

Wang, Z. Y., Wang, D. Y., Smith, S. T., and Lu, D. G. (2012b). CFRP-Confined square RC columns. I: Experimental investigation. *J. Compos. Constr.* 16, 150–160. doi:10.1061/(asce)cc.1943-5614.0000245

Woldemariam, A. M., Oyawa, W., and Nyomboi, T. (2019). Behavior of concrete-filled single and double-skin uPVC tubular columns under axial compression loads. *open Constr. Build. J.* 13, 164–177. doi:10.2174/1874836801913010164

Woldemariam, A. M., Oyawa, W. O., and Nyomboi, T. (2019). Structural performance of uPVC confined concrete equivalent cylinders under axial compression loads. *Buildings* 9 (4), 82. doi:10.3390/buildings9040082

Xiao, Y. (2004). Applications of FRP composites in concrete columns. *Adv. Struct. Eng.* 7 (4), 335–343. doi:10.1260/1369433041653552

Xu, Y., Tang, H., Chen, J., Jia, Y., and Liu, R. (2021). Numerical analysis of CFRP-confined concrete filled stainless steel tubular stub columns under axial compression. *J. Build. Eng.* 37, 102130. doi:10.1016/j.jobe.2020.102130

Yu, F. (2007). "Experimental Study and theoretical analysis on mechanical behavior of PVC–FRP confined concrete column," (Xi'an: University of Architecture and Technology). Doctoral thesis.

Yu, F., Zhang, N., Niu, D., Kong, Z., Zhu, D., Wang, S., et al. (2019). Strain analysis of PVC-CFRP confined concrete column with ring beam joint under axial compression. *Compos. Struct.* 224, 111012. doi:10.1016/j.compstruct.2019.111012

Zhang, H., and Hadi, M. N. S. (2020). Geogrid-confined pervious geopolymer concrete piles with FRP-PVC confined concrete core: Analytical models. *Structures* 23, 731–738. doi:10.1016/j.istruc.2019.11.005

Nomenclature

Ac the cross-sectional area of concrete core (mm^2)

Ag cross-sectional area of concrete column (mm^2)

CFST Concrete Filled Steel Tubes

CFPT Concrete Filled PVC Tubes

RC Reinforced Concrete

FE Finite Element

$\mathbf{f_{cc}}$ Confined Concrete compressive strength (MPa)

$\mathbf{f_{co}}$ Unconfined Concrete compressive strength (MPa)

t thickness of PVC tube (mm)

D Diameter of the PVC tube (mm)

L/H Length/height of the PVC tube (mm)

$\mathbf{f_{cc}/f_{co}}$ confined concrete compressive strength to unconfined concrete compressive strength ratio

$\mathbf{D_c}$ Diameter of the concrete core without PVC tube (mm)

$\mathbf{f_c'}$ strength of unconfined concrete cylinder under compression (MPa)

$\mathbf{\varepsilon_{EP}}$ Peak experimental strain (mm/mm)

$\mathbf{\varepsilon_{FP}}$ Peak finite element modeling strain (mm/mm)

$\mathbf{P_{EP}}$ Peak Experimental Load (kN)

$\mathbf{P_{FP}}$ Peak finite element modeling Load (kN)

CDPM Concrete Damaged Plastic Model

$\mathbf{\Psi}$ dilation angle

Kc Shape factor for the yielding surface

e plastic flow potential eccentricity

$\mathbf{\mu}$ Viscosity Parameter

$\mathbf{f_{bo}/f_c'}$ ratio of biaxial stress to uniaxial stress

$\mathbf{f_c''}$ considered to be 80% of the concrete cylinder strength (MPa)

$\mathbf{\varepsilon_{cc1}}$ the strain of the confined concrete at the first peak load

$\mathbf{\varepsilon_{c0}}$ 0.002 for unconfined concrete strength at peak load

$\mathbf{k_{es}}$ the ratio of effectively confined concrete area to the confined area

$\mathbf{f_{yt}}$ the yield strength of the steel

AAE Average Absolute Error

$\mathbf{f_l}$ yield stress of longitudinal steel reinforcement (mm^2)

$\mathbf{f_h}$ yield stress of hoop steel reinforcement (mm^2)

$\mathbf{f_{pvc}}$ yield stress of pvc (mm^2)

Ec Young's modulus of concrete (MPa)

$\mathbf{\lambda_{pvc}}$ dimensionless parameter for the PVC

$\mathbf{\lambda_h}$ dimensionless parameter for the hoop reinforcement

$\mathbf{\lambda_l}$ dimensionless parameter for the longitudinal reinforcement

$\mathbf{\rho_{ls}}$ volumetric ratio for the longitudinal reinforcement

$\mathbf{\rho_{hs}}$ volumetric ratio for the hoop reinforcement

MCR Modified Confined Pressure Ratio (MCR)